Free Energies of Formation of Metal Clusters and Nanoparticles from Molecular Simulations: Al_n with $n = 2-60$

Zhen Hua Li, Divesh Bhatt, Nathan E. Schultz, J. Ilja Siepmann,* and Donald G. Truhlar*

Department of Chemistry and Supercomputing Institute, University of Minnesota, Minneapolis, Minnesota 55455-0431

Received: May 9, 2007; In Final Form: July 30, 2007

Efficient simulation methods are presented for determining the standard Gibbs free energy changes for the reactions, $M + M_{n-1} \leftrightarrow M_n$ (R1), involved in the formation of atomic clusters and nanoparticles (also called particles) in the vapor phase. The standard Gibbs free energy of formation ($\Delta_f G°$) of a particle is obtained from these Gibbs free energy changes ($\Delta G°$) by a recursion relationship using the experimental $\Delta_f G°$ of the monomer. In the present study, this method has been applied to reactions involving Al_n particles with $n = 2-60$. This method has been validated for $n = 2$, where the experimental thermodynamic properties of Al_2 have been recompiled using the latest available experimental or highly accurate theoretical data. For $n = 2-4$, two completely different approaches, a Monte Carlo configuration integral (MCCI) integration of partition functions and a Monte Carlo direct simulation of the equilibrium constants (MCEC), employing four well-validated potential energy functions have been used to calculate $\Delta G°$ of R1. Excellent agreement is observed for these two methods. Although different potential energy functions give different stage-1 results for $n \leq 10$, three high-level correction (HLC) terms, namely, a correction for the potential energy difference of the global minima, another for the electronic excitation contribution, and a third based on calculating isomeric−rovibrational contribution, have been applied to mitigate deficiencies in the potential energy functions. For $n = 2$, good agreement has been found between the corrected simulation results and experimental data. For larger n, the more efficient MCEC method has been used. Finally, accurate $\Delta G°$ of R1 and thus $\Delta_f G°$ of Al_n particles with $n = 2-60$ have been determined. This is the first example of the determination of nanoparticle free energies of formation.

1. Introduction

Metal nanoparticles have unique electrical, optical, magnetic, chemical, and catalytic properties that have attracted interest for a wide variety of applications.[1,2] In order to understand and exploit these properties, it is necessary to control particle size and shape during synthesis. The key thermodynamic variable affecting the size distribution is the free energy as a function of particle size, but, because of the difficulty of carrying out size-selective thermodynamic measurements, this function is not known for any species in the nanoparticle regime.

Aluminum nanoparticles have potential applications as an ingredient for high-energy fuels such as rocket propellants[3−5] and as a hydrogen storage device.[6] Assessing the prospects for such uses requires a detailed knowledge of the thermodynamics and kinetics of the growth of nanoparticles. In the present work, the standard Gibbs free energies of formation of Al clusters and nanoparticles (Al_n with $n = 2-60$) are determined through the calculation of the standard Gibbs free energy change ($\Delta G°(n)$) of the following reaction:

$$Al + Al_{n-1} \rightarrow Al_n \qquad \text{(R1)}$$

Quasispherical face-centered-cubic Al_n particles with $n = 19$ and 55 have diameters of about 1.4 and 2.0 nm, respectively.[7] Thus, we say "cluster" for $n = 2-19$, "nanoparticles" for $n = 20-60$, and "particles" to refer to either. Reaction R1 itself is very important in the vapor-phase growth of the Al_n clusters and nanoparticles via addition of individual atoms to an existing particle, which is the dominant set of elementary steps in the condensation/evaporation mechanism.

Once $\Delta G°(n)$ of R1 is calculated, the standard free energy of formation $\Delta_f G°(n)$ of Al_n particles can then be obtained by the following recursion relationship:

$$\Delta_f G°(n) = \Delta G°(n) + \Delta_f G°(n-1) + \Delta_f G°(1) \qquad (1)$$

where $\Delta_f G°(1)$ is the standard free energy of formation of Al monomer, which is known for an ideal gas.[8]

In the present work, $\Delta G°(n)$ of R1 is obtained both by directly simulating the equilibrium constant and by calculating the partition functions of the reactants and products by evaluation of their configuration integrals. Both methods employ analytic potential energy functions. Two of these analytic potential energy functions were developed previously,[7] and two are new in this work. The functions were validated against PBE0[9] density functional theory (DFT) calculations for aluminum clusters and nanoparticles and against experimental bulk properties of aluminum;[7,10] furthermore, PBE0 and the basis sets used for these calculations were validated against higher-level theory for small systems.[11] Recently, these potential energy functions have been demonstrated to give a good representation of the vapor−liquid coexistence properties of Al from the triple point to the critical temperature.[12]

This manuscript is organized as follows. In Section 2, we describe the different potential energy functions and the distance

* Corresponding authors. E-mail: siepmann@chem.umn.edu (J.I.S.) and truhlar@umn.edu (D.G.T.).

10.1021/jp073559v CCC: $37.00
Published on Web 10/11/2007

criterion used to define whether an atom belongs to a particle. The simulation methods employed for the calculations of the equilibrium constants as functions of particle size are presented in Section 3. These equilibrium constants are fully coupled (i.e., nonseparable) classical ones corresponding to the most accurate analytic potential for $n = 3-10$ and a more affordable one for $n \geq 11$. Section 4 describes corrections for higher-level potentials and for including quantal effects, in particular, electronic excitation and quantized vibrations. In Section 6, the simulation results are discussed separately for small particles consisting of two to four atoms and for larger particles consisting of five or more atoms. Finally, we conclude with a summary of the most important findings.

2. Potential Energy Functions

Two previously developed analytic potentials[7,10] for aluminum are used in this work, namely, potentials NP-A and NP-B. NP-A is probably the most accurate analytic potential currently available that is applicable from gas-phase dimers to condensed phases.[7] NP-B is slightly less accurate than NP-A but is at least an order of magnitude less expensive to evaluate.

The NP-A and NP-B potential energy functions were refined in this work to obtain better potentials for small clusters. Specifically, we re-optimized these potentials using the data sets for the four smallest clusters (Al_2, Al_3, Al_4, and Al_7) in our large database that has been described previously.[7] The re-optimized potentials are called NP-A-2347 and NP-B-2347. The mean unsigned errors (MUEs) for the four data sets and the reoptimized parameters are given in Supporting Information. For the NP-A potential, the parameters of the pairwise term were first fitted accurately to dimer data with a MUE of 0.013 eV/atom, and then the dimer parameters were fixed during the fitting to the whole dataset. Therefore, the NP-A and NP-A-2347 results for the dimer presented in this study are exactly the same, and we refer to them simply as NP-A results.

Atoms that are less than a certain distance (called the particle criterion) away from one another are considered to be parts of the same particle. All of the potentials used in this work contain a cutoff distance r_c, beyond which two atoms do not interact with each other, and this cutoff is used as the particle criterion. It equals 6.50 Å for NP-A and NP-A-2347, and it equals 5.38 Å for NP-B and NP-B-2347. In principle, the cluster size distribution must depend on the value r_c; for example, if the value of r_c were chosen to be much less than the Al−Al bond length, then only monomers would be inferred to be present, or if the value of r_c were chosen to be much too large (say, half the box length), then all atoms would be considered to be part of a single large cluster. However, there is a range of r_c values (usually close to the position of the first minimum in the radial distribution function for the condensed phase) over which the cluster size distribution and the Gibbs free energy are relatively insensitive to changes in r_c. In this work, we validated that r_c values of 4.0 and 4.8 Å yield cluster size distributions that agree with those obtained for the standard $r_c = 5.38$ to within the statistical uncertainty (see Figure S4 in Supporting Information).

3. Simulation Methods

3.1. Partition Function Methods. $\Delta G^\circ(n)$ of R1 can be calculated from the canonical molecular partition functions of the reactants and products by

$$\Delta G^\circ(n) = \Delta E_e(n) - RT \ln \frac{Q(n)/N_A}{[Q(n-1)/N_A][Q(1)/N_A]} \quad (2)$$

where N_A is the Avogadro constant, $\Delta E_e(n)$ is the potential energy change of R1 with all reagents at their classical equilibrium structures, which are taken as reference structures, and Q is the canonical total partition function of a particle with the zero of energy at the reference structure.

$$Q(n) = q_{Trans} \sum_{\eta,\gamma,\upsilon,j} g_{\eta,\gamma,\upsilon,j}\, e^{-\beta(E_{\eta,\gamma}+\epsilon_{\eta,\gamma,\upsilon,j})} \quad (3)$$

where q_{Trans} is the translational partition function; $E_{\eta,\gamma}$ is the minimum potential energy of isomer γ in electronic state η relative to that of the global minimum (which is the global reference structure); $\epsilon_{\eta,\gamma,\upsilon,j}$ is the rovibrational energy level (relative to $E_{\eta,\gamma}$) of the state with vibrational quantum numbers υ and rotational quantum numbers j in electronic state η for isomer γ; $g_{\eta,\gamma,\upsilon,j}$ is the degeneracy of the state of isomer γ with quantum numbers η, υ, and j; and $\beta = 1/kT$ where k is the Boltzmann constant and T is the absolute temperature. If the isomeric−rovibrational energies ($\epsilon_{\eta,\gamma,\upsilon,j}$) are the same for all electronic states (which is called the electronic separable approximation[13−15]), then

$$Q(n) = q_{Trans} \sum_{\eta} g_\eta\, e^{-\beta E_\eta} \sum_{\gamma,j,\upsilon} g_{\gamma,\upsilon,j}\, e^{-\beta(E_\gamma+\epsilon_{\gamma,j,\upsilon})} \equiv q_{Trans} q_{Elec} q_{IsoRov} \quad (4)$$

where g_η is the electronic degeneracy; $g_{\gamma,\upsilon,j}$ is the degeneracy of the nuclear-motion wave function for state γ, υ, j; the first sum over η is the electronic partition function (q_{Elec}), and the second sum is the isomeric−rovibrational partition function (q_{IsoRov}),[16]

$$q_{IsoRov} = \sum_\gamma q_{Rov}^{(\gamma)}\, e^{-\beta E_\gamma} \quad (5)$$

where $q_{Rov}^{(\gamma)}$ is the rovibrational partition function of isomer γ. If a molecule has only one isomer, q_{IsoRov} reduces to the usual rovibrational partition function q_{Rov}.

In classical mechanics, the isomeric−rovibrational partition function for a classical N-atom particle is

$$Q_{IsoRov} = \frac{C}{\Lambda^{3N-3} N!} \quad (6)$$

where C is the configuration integral (CI)

$$C = \int d\mathbf{r}_1\, d\mathbf{r}_2 \cdots d\mathbf{r}_N\, \delta(\mathbf{r}_{com})\, e^{-\beta U} \quad (7)$$

in which the integration is over all atomic coordinates, the delta function restricts the center of mass to be at the origin, U is the potential energy of a given configuration, and Λ is the thermal de Broglie wavelength given by

$$\Lambda = \frac{h}{\sqrt{2\pi M k T}} \quad (8)$$

where h is Planck's constant, and M is the mass of an atom.

Since the analytic potentials used are developed for the electronic ground state of the aluminum systems, the simulations with these analytic potentials do not give information about q_{Elec}, which is set equal to unity in the rest of this section. The electronic partition function depends on n and will be discussed in Section 4.

3.1.1. Direct Configuration Integral (DCI). Al_2 has only one isomer, thus q_{IsoRov} reduces to q_{Rov}. The classical q_{Rov} of a diatomic molecule can be calculated by a direct integration of

the configuration integral (DCI).[17] The result, including the quantum mechanical symmetry factor, is

$$q_{\mathrm{Rov}} = \frac{8\pi^2}{\sigma h^3}(2\mu/\beta)^{3/2}\int_B \mathrm{e}^{-\beta u(r)}\left\{\frac{\sqrt{\pi}}{2}\,\mathrm{erf}[\sqrt{-\beta u(r)}] - \sqrt{-\beta u(r)}\,\mathrm{e}^{\beta u(r)}\right\} r^2\,\mathrm{d}r \quad (9)$$

where σ is the rotational symmetry number (2 for Al_2), μ is the reduced mass, $u(r)$ is the potential energy relative to the dissociation limit, and the integration is over the bonded region, from the inner bond distance, where $u(r) = 0$, to the cutoff distance of the analytic potentials. Equation 9 is based on an energy constraint as well as a distance constraint to separate the diatomic region of phase space from the dissociated region, but in the subsequent work below, we use only a distance constraint.

3.1.2. Monte Carlo Configuration Integral (MCCI) Methods. For $n = 3$ and 4, isomeric−rovibrational partition functions are calculated by computing the classical CIs[14] by Monte Carlo integration over all space with uncorrelated stratified sampling[18,19] and importance sampling[19,20] using the FPIMC computer program.[21] This method is also applied for $n = 2$ as a check. The isomeric−rotational/vibrational partition function of a molecule is given by

$$q_{\mathrm{Rov}} = \frac{1}{\sigma h^{3N-3}}\int \mathrm{d}\mathbf{x}\,\mathrm{d}\mathbf{p}\,\delta(\mathbf{r}_{\mathrm{com}})\exp(-\beta U(\mathbf{x})) \quad (10)$$

where $\mathbf{x}$ denotes atomic coordinates, $\mathbf{p}$ denotes their conjugate momenta, and $U(\mathbf{x})$ is the potential energy at point $\mathbf{x}$ relative to the global minimum. Equation 10 is evaluated by Monte Carlo sampling. It should be noted that if the integration in eq 10 is over all bonded regions of a multiple-isomer molecule (see the definition of a particle in Section 2), the q_{Rov} given by eq 10 is q_{IsoRov} (eq 5).

3.2. Monte Carlo Equilibrium Constant (MCEC) Methods. Using the particle criterion introduced in Section 2 and defining a pair potential $u(r_{ij})$ such that U tends to $u(r_{ij})$ when atoms i and j are in a dimer, we find the partition function for an N-atom system containing multiple particles and monomers can be written as

$$Q_{\mathrm{System}} = \frac{1}{\Lambda^{3N}N!}\left[\frac{N(N-1)}{2}\int_{\substack{r_{12}<r_c;r_{ij}>r_c;\\ ij\neq 12}} \mathrm{e}^{-\beta u(r_{12})}\,\mathrm{d}\mathbf{r}_1\cdots\mathrm{d}\mathbf{r}_N + \int_{\substack{r_{ij}>r_c;\\ ij\neq 12}} \mathrm{d}\mathbf{r}_1\cdots\mathrm{d}\mathbf{r}_N + \text{other terms}\right] \quad (11)$$

where the first integral is over one dimer and $N - 2$ monomers, the second integral is over N monomers, and the "other terms" include larger particles as well as 2 dimers and $N - 4$ monomers and so on. The factor $N(N - 1)/2$ represents the number of ways one dimer can be picked in an N-atom system.

In the limiting case when only the monomers and dimers are present in non-negligible amounts in the system, and, moreover, when the concentration of monomers is much larger than that of dimers, only the two explicit terms in eq 11 contribute significantly to the partition function. Intuitively, as can also be observed from explicit simulations, such a limiting case can be realized for systems with very large volumes, since the entropic penalty for the formation of particles (dimers and larger) increases with the volume.

For such a limiting case, eq 11 simplifies to

$$Q_{\mathrm{System}} \approx \frac{V^{N-1}}{\Lambda^{3N}N!}\left[\frac{N(N-1)}{2}4\pi\int_{r<r_c} r^2\,\mathrm{e}^{-\beta u(r)}\,\mathrm{d}r + V\right] \quad (12)$$

In writing eq 12, we have assumed that the volume accessible to each of the N monomers (i.e., all distances are greater than r_c) is still V. Such an assumption is appropriate for the limiting case mentioned above.

The ratio of the two terms in eq 12 gives the ratio of the number of times the system has all monomers and the number of times it has 1 dimer and $N - 2$ monomers. Thus, if the fraction of times a dimer is seen in the system is n_2 (which equals the fraction of times that 1 dimer and $N - 2$ monomers are present in the system), the ratio of the probability that the system is in the all-monomer state to the probability that it contains exactly 1 dimer and $N - 2$ monomers is

$$\frac{1-n_2}{n_2} = \frac{V}{2\pi N(N-1)\int_{r<r_c} r^2\,\mathrm{e}^{-\beta u(r)}\,\mathrm{d}r} \quad (13)$$

This equation, along with the condition that the total number of atoms is N, can be solved to yield n_2, and, hence, the monomer and dimer concentrations at equilibrium. In the ideal-gas limit, the equilibrium constant is obtained as

$$K_{\mathrm{C}} \equiv \frac{[\mathrm{Al_2}]}{[\mathrm{Al}]^2} = \frac{2\pi(N-1)\int_{r<r_c} r^2\,\mathrm{e}^{-\beta u(r)}\,\mathrm{d}r}{N} \quad (14)$$

In eq 14, a further limiting assumption that $V \gg 2\pi(N-1)(N-2)\int_{r<r_c} r^2\,\mathrm{e}^{-\beta u(r)}\,\mathrm{d}r$ is used. All of the above restrictions of large V are consistent with the ideal-gas limit in which the equilibrium constant of eq 14 is meaningful. In the limit of large N, eq 14 further reduces to

$$K_{\mathrm{C}} \equiv \frac{(Q_{\mathrm{Al_2}}/V)}{(Q_{\mathrm{Al}}/V)^2} = 2\pi\int_{r<r_c} r^2\,\mathrm{e}^{-\beta u(r)}\,\mathrm{d}r \quad (15)$$

Equation 15 can be used to determine whether the simulations are performed for a dilute enough gas to get a reliable estimate of the equilibrium constant. Equation 14 stipulates that the number of atoms in the simulations must be large enough, in addition to the volume being large, to get the correct results for the free energies of formation. Furthermore, eq 14 provides a way of ascertaining the number of atoms in the classical simulations that are large enough to give the accurate standard free energy changes within the simulation error as well as the uncertainty of the analytic potentials.

The equilibrium constant and the corresponding standard Gibbs free energy change can, in principle, be obtained via canonical ensemble simulations of a very dilute (ideal) gas as mentioned above. Aggregation-volume-bias Monte Carlo (AVB-MC) methods[22,23] can be used for efficient sampling of particle formation and breakage. However, only a small range of particle sizes can be found in unbiased canonical simulations of a dilute gas because of the large free energy penalty for larger particles. Frenkel and ten Wolde[24] used a biasing potential, dependent upon the size of the largest particle, to simulate a wide range of particle sizes of a Lennard-Jones fluid. A similar biasing scheme was subsequently used by Chen et al. in the isobaric−isothermal and grand-canonical ensembles.[25,26] Accordingly, the potential energy of the system is replaced by $U_{\mathrm{b}} = U + W(N_{\mathrm{c}})$, where W is the biasing potential that depends upon the size,

N_c, of the largest particle in the system. However, in previous simulations, a seed particle was used to define a particle, and the bias acted only on that particular particle.

3.2.1. AVBMC-A. In this method, denoted AVBMC-A where A denotes "any" particle (see below), canonical ensemble simulations are performed with a biasing potential that depends upon the size of the largest particle present in the system. In addition to regular translational moves, we use an AVBMC move that transfers atom *j* to the vicinity of atom *i*, and we use the reverse move (called AVBMC-2 by Chen and Siepmann[23]). In contrast to Chen et al. in their nucleation work,[25] atom *i* is any atom in the system and not necessarily in the largest particle. Accordingly, the acceptance probability of moving *j*, outside the vicinity of *i*, to the vicinity of *i* is given by

$$P_{acc} = \min\left[1, \frac{(1-P_{bias})V_{in}N_{out}}{P_{bias}V_{out}(N_{in}+1)} \times e^{-\beta\Delta U}\, e^{-\beta(W(N_{c,new})-W(N_{c,old}))}\right] \quad (16)$$

where P_{bias} is the probability that an out → in move is chosen (i.e., *j* is moved from the out region of *i* to the in region), V_{in} is the volume of the in region of *i*, V_{out} is the volume of the box excluding the in region of *i*, N_{in} and N_{out} are the number of atoms in the in and the out regions of *i*, respectively, and $N_{c,new}$ and $N_{c,old}$ are the sizes of the largest particle in the system in the new and the old configurations, respectively.

Similarly, the acceptance probability of the reverse move, moving *j* from within the vicinity of *i* to outside, is given by

$$P_{acc} = \min\left[1, \frac{P_{bias}V_{out}N_{in}}{(1-P_{bias})V_{in}(N_{out}+1)} \times e^{-\beta\Delta U}\, e^{-\beta(W(N_{c,new})-W(N_{c,old}))}\right] \quad (17)$$

The two acceptance probabilities in eq 16 and 17 are the AVBMC2 acceptance probabilities derived by Chen and Siepmann.[23]

3.2.2. AVBMC-L. In the second method, called AVBMC-L where L denotes "largest", the target atom *i* is chosen to be inside the largest particle. This changes the acceptance probabilities. For the forward move, one obtains

$$P_{acc} = \min\left[1, \frac{(1-P_{bias})V_{in}(N-N_{c,old})}{P_{bias}V_{out}(N_{in}+1)} \times e^{-\beta\Delta U}\, e^{-\beta(W(N_{c,new})-W(N_{c,old}))}\frac{N_{c,old}}{N_{c,new}}\right] \quad (18)$$

and similarly for the reverse move, one obtains

$$P_{acc} = \min\left[1, \frac{P_{bias}V_{out}N_{in}}{(1-P_{bias})V_{in}(N-N_{c,old}+1)} \times e^{-\beta\Delta U}\, e^{-\beta(W(N_{c,new})-W(N_{c,old}))}\frac{N_{c,old}}{N_{c,new}}\right] \quad (19)$$

In both eqs 18 and 19, V_{out} is the volume of the box excluding the combined volume of the in region of *i* and the largest particle of which *i* is a part of. In contrast to AVBMC-A, *i* is chosen from the largest particle present in the system. This is accounted for by the ratio of the sizes of the largest particles in the old and the new configuration appearing in eqs 18 and 19. These equations resemble those used by Chen et al., except for the fact that the biasing potential depends on the size of the largest particle present in the system. Since the largest particle may change because of the in → out move, care must be taken to maintain detailed balance. Thus, the AVBMC2 moves that lead to switching the identity of the largest particle are rejected in this formalism. It is not necessary to subject regular translational moves to this requirement because all *N* atoms are equally likely to be picked for translation.

An advantage of AVBMC-L is that AVBMC moves are performed explicitly on the largest particle present in the system, and it is, therefore, more efficient than AVBMC-A in simulating particles of different sizes. However, the volume of the largest particle, as present in the acceptance probabilities of AVBMC-L, cannot be calculated in a straightforward manner and is neglected in the simulations. Although the volume of the particle is much smaller than the volume outside the particle, a comparison of AVBMC-L with the neglected particle volume and the exact AVBMC-A provides a test for the effect of neglecting the particle volume.

Unweighted canonical ensemble averages for any observable *A*, can be obtained from these biased Monte Carlo simulations as

$$\langle A \rangle = \frac{\langle A\, e^{\beta W}\rangle_b}{\langle e^{\beta W}\rangle_b} \quad (20)$$

where the subscript *b* denotes averages in the biased simulations.

4. High-Level Corrections

Three sources of inaccuracy in the results obtained by the methods described in Sections 2 and 3 are remediated by adding correction terms. This yields

$$\Delta G^{\circ}_{Acc}(n) = \Delta G^{\circ}(n) + \Delta\Delta E_e^{HLC}(n) + \Delta G_{Elec}(n) + \Delta G_{IsoRov}^{HLC}(n) \quad (21)$$

where $\Delta G^{\circ}(n)$ is the "stage-1" result obtained by the classical methods of Section 3 with an analytic potential of Section 2, and the next three terms are the corrections. These are discussed in the next three subsections.

4.1. Electronic Structure Correction. The first correction is

$$\Delta\Delta E_e^{HLC}(n) = \Delta E_e^{HL}(n) - \Delta E_e^{LL}(n) \quad (22)$$

where the subscript "e" denotes a classical equilibrium geometry, and ΔE_e^{LL} and ΔE_e^{HL} are the potential energy changes during process R1 predicted by the analytic potential (low level, LL) and a high-level (HL) method, respectively. In the present work, for $n \le 7$, the high level results are calculated by exponentially extrapolating[27] single-point CCSD(T)/aug-cc-PV*n*Z//QCISD/6-31+G(d) (n = D, T, Q) energies to the complete basis set limit, and this method is denoted as CC/CBS. For $8 \le n \le 13$, PBE0/MG3[28] geometries and energies are used. For $14 \le n \le 30$, PBE0/MEC geometries and energies were used. For $31 \le n \le 60$, single-point PBE0/MEC[29] energies using NP-A global minimum geometries were used. For large particles, an extensive searching for the global minima is very expensive using density functional methods. Therefore, for particles with $n = 8-19$, we start from the known global minimum structures in the literature, where available,[30−33] and reoptimize them. Otherwise, the geometries searched using the NP-B potential[16] were reoptimized using the NP-A potential to determine the global minima at NP-A level and using them as the starting geometry

for the PBE0 geometry optimization. Harmonic vibrational frequencies were calculated after geometry optimization to check if the optimized geometry is a local minimum. For each particle, the two lowest spin states, singlet and triplet for particles with even number of electrons and doublet and quartet for particles with odd number of electrons, were considered to determine the electronic ground state.[31,32] Full geometry optimizations with PBE0 method were carried out for the two lowest spin states of the particles with $n = 2-30$.

4.2. Electronic Excitation Correction. As mentioned in conjunction with eq 4, the electronic partition function is not included in the results obtained by the analytic potentials; q_{Elec} is obtained by a sum over all of the electronic states (see eq 4). The contribution of the electronic partition function to the Gibbs free energy of a particle is

$$G_{\mathrm{Elec}}(n) = -kT \ln q_{\mathrm{Elec}}(n) \tag{23}$$

and the contribution to the free energy change of R1 is

$$\Delta G_{\mathrm{Elec}}(n) = -kT \ln \frac{q_{\mathrm{Elec}}(n)}{q_{\mathrm{Elec}}(n-1)\, q_{\mathrm{Elec}}(1)} \tag{24}$$

To converge q_{Elec} for high-temperature metal particles requires many electronic states. Unfortunately, as the size of the particle grows, it quickly becomes impractical to calculate all of these states because q_{Elec} grows exponentially. An alternative way to calculate the contribution of the electronic partition function to thermodynamic properties is to assume that electrons are distributed in the Kohn−Sham orbitals by Fermi−Dirac statistics.[35−37] With this scheme, the thermal electronic energy is

$$E_{\mathrm{Elec}}(n) = \sum_i \sum_{\lambda=\alpha,\beta} f_{i,\lambda}\epsilon_{i,\lambda} \tag{25}$$

where the first sum is over all orbital energy levels for orbital spin λ, and f is the Fermi-Dirac occupation number

$$f_{i,\lambda} = (1 + \mathrm{e}^{(\epsilon_{i,\lambda}-\mu)/kT})^{-1} \tag{26}$$

where μ is the chemical potential which is determined from the particle conservation equation

$$\sum_i \sum_\lambda f_{i,\lambda} = N_{\mathrm{e}} \tag{27}$$

where N_{e} is the total number of electrons. The electronic entropy $S_{\mathrm{Elec}}(n)$ is given by

$$S_{\mathrm{Elec}}(n) = -k\sum_i \sum_\lambda [f_{i,\lambda} \ln f_{i,\lambda} + (1 - f_{i,\lambda}) \ln(1 - f_{i,\lambda})] + k \ln g_0 \tag{28}$$

where g_0 is the degeneracy of the ground electronic state. The electronic excitation contribution to Gibbs free energy is then calculated by

$$G_{\mathrm{Elec}}(n) = E_{\mathrm{Elec}}(n) - TS_{\mathrm{Elec}}(n) \tag{29}$$

The corresponding correction to the free energy change of R1 is

$$\Delta G_{\mathrm{Elec}}(n) = G_{\mathrm{Elec}}(n) - [G_{\mathrm{Elec}}(n-1) + G_{\mathrm{Elec}}(1)] \tag{30}$$

In the present study, eqs 23 and 24 were used with many-electron energy levels E_η calculated by time-dependent density functional theory[34−39] (TD−DFT) for $n = 2-20$, and eqs 25−30 were used for $n > 20$. The TD−DFT excitation energies for $n = 2-10$ were calculated at the TD-PBE0/MG3 level, and those for $n = 11-20$ were calculated at the TD-PBE0/MEC level. For each particle with $n \le 20$, the geometries of the lowest two spin states were fully optimized at the same level used for calculating excitation energies. Excitation energies of higher spin states, up to multiplicity 11 if n is even and 12 if n is odd (except for Al_2 and Al_3, for which only valence electron excitations were considered), were calculated using the geometry of the triplet or quartet spin state. At least 200 excitation energies were calculated for the electronic ground state to guarantee that q_{Elec} is converged, where excitation energies up to 2.4 eV are needed for Al_{20} to converge q_{Elec} at 3000 K. For $n > 20$, the orbital energies used are from the electronic ground state at the PBE0/MEC level.

All electronic calculations were performed without symmetry and with the spin-unrestricted formalism (UPBE0). Because of symmetry breaking, the electronic degeneracies are usually unity, in which case $G_\eta = 2S + 1$, where S is the total electronic spin quantum number.

4.3. Isomeric−Rovibrational Corrections. Although the present simulations using the DCI, MCCI, and MCEC methods do not involve separate contributions of different isomers and their rotations and vibrations, these separable contributions may be used to correct the calculations with $n \ge 10$, which use the NP-B potential, for the fact that NP-B is less accurate than NP-A. We include the nonseparable calculations of Section 3 in the first term on the right-hand side of eq 21, but we use a partially separable approximation involving E_γ and $\epsilon_{\gamma,j,\upsilon}$ for a high-level correction. This is accomplished by optimizing the geometry of each low-energy isomer and then, still assuming nonseparable isomeric energies, calculating separable vibrational modes for each isomer. The further assumption is made that the rotational ($q_{\mathrm{Rot}}^{(\gamma)}$) and vibrational ($q_{\mathrm{Vib}}^{(\gamma)}$) partition functions are separable in eq 5.[16] The former is calculated classically using a rigid-rotor (RR) approximation as

$$q_{\mathrm{Rot}}^{(\gamma)} = \left(\frac{8\pi^3 kT}{h^2}\right)^{f_{\mathrm{Rot}}^{(\gamma)}/2} \frac{\prod_i^{f_{\mathrm{Rot}}^{(\gamma)}} \sqrt{I_i^{(\gamma)}}}{\sigma^{(\gamma)}\pi} \tag{31}$$

where $\{I_i^{(\gamma)}\}$ are the principal moments of inertia, $\sigma^{(\gamma)}$ is the rotational symmetry number, and $f_{\mathrm{Rot}}^{(\gamma)}$ is the number of rotational degrees of freedom which is 3 for nonlinear structures and 2 for linear structures. To obtain $\sigma^{(\gamma)}$, one needs to know the point group of every isomer. This is done by running a short Gaussian 03[40] job with a loose criterion on judging the symmetry of molecules (keyword symm=loose) using the geometry of the isomer and stopping the program at link 202. Then, we extract the point group out from the output. Using the harmonic-oscillator (HO) approximation, we find the quantum mechanical expression for $q_{\mathrm{Vib}}^{(\gamma)}$ is

$$q_{\mathrm{Vib}}^{(\gamma)} = \prod_m \frac{\mathrm{e}^{-1/2h\omega_m^{(\gamma)}/kT}}{1 - \mathrm{e}^{-h\omega_m^{(\gamma)}/kT}} \tag{32}$$

where $\omega_m^{(\gamma)}$ is the vibrational frequency of mode m of isomer γ. The classical expression for $q_{\mathrm{Vib}}^{(\gamma)}$ is

$$q_{\mathrm{Vib}}^{(\gamma)} = \prod_m \frac{kT}{h\omega_m^{(\gamma)}} \quad (33)$$

The high-level multiplicative correction factor for the isomeric−rovibrational partition function is then given by

$$f_{\mathrm{IsoRov}}^{\mathrm{HLC}}(n) = \frac{q_{\mathrm{IsoRov}}^{\mathrm{HL}}(n)}{q_{\mathrm{IsoRov}}^{\mathrm{LL}}(n)} \quad (34)$$

where q_{IsoRov} (defined by eq 5) is calculated with the separable approximation on $q_{\mathrm{Rot}}^{(\gamma)}$ and $q_{\mathrm{Vib}}^{(\gamma)}$ using the RR-HO approximation described above. To calculate q_{IsoRov}, the sum in eq 5 is carried out over all of the low-energy isomers (up to a maximum of 2000 isomers) located in the previous work by the NP-B potential,[16] and all of these isomer geometries are reoptimized using the NP-A potential to calculate $q_{\mathrm{IsoRov}}^{\mathrm{HL}}$. Since the simulation is done classically, the low-level $q_{\mathrm{Vib}}^{(\gamma)}$ is calculated using eq 33, while high-level $q_{\mathrm{Vib}}^{(\gamma)}$ is calculated using eq 32. The correction to $\Delta G^{\circ}(n)$ is then given by

$$\Delta G_{\mathrm{IsoRov}}^{\mathrm{HLC}}(n) = -RT \ln(f_{\mathrm{IsoRov}}^{\mathrm{HLC}}(n)/f_{\mathrm{IsoRov}}^{\mathrm{HLC}}(n-1)) \quad (35)$$

Large particles have many low vibrational frequencies, and they make a large contribution to $q_{\mathrm{Vib}}^{(\gamma)}$ at high temperatures. However, $q_{\mathrm{Vib}}^{(\gamma)}$ calculated using the HO approximation with these very low frequencies may be overestimated because of anharmonicity. For very low frequencies, the harmonic approximation typically predicts a motion of much wider amplitude than is allowed to be sampled by an accurate anharmonic potential.[41] Therefore, a reasonable but simple way to improve the harmonic calculation of $q_{\mathrm{Vib}}^{(\gamma)}$ is to raise any vibrational frequencies below a certain value, to a cutoff frequency called ω_{cut}. We have therefore raised all frequencies below ω_{cut} to ω_{cut}. We have tested three choices of ω_{cut}, namely, 70, 100, and 130 cm^{-1}. A larger ω_{cut} results in a smaller absolute value of $\Delta G_{\mathrm{IsoRov}}^{\mathrm{HLC}}(n)$ (see also Figure S2 of Supporting Information). The maximum deviation between the values calculated using the three ω_{cut} values is 7 kcal/mol. The mean absolute deviations of the $\Delta G_{\mathrm{IsoRov}}^{\mathrm{HLC}}(n)$ values calculated with $\omega_{\mathrm{cut}} = 100$ cm^{-1} from those with $\omega_{\mathrm{cut}} = 130$ cm^{-1} and 70 cm^{-1} are only 1.0 and 1.5 kcal/mol. On the basis of our estimate of what value will best account for anharmonicity, we chose $\omega_{\mathrm{cut}} = 100$ cm^{-1} for all the rest of the calculations.

4.4. Consistency. To reduce systematic error, for each correction, the same method is used for both Al_n and Al_{n-1}; for example, to calculate $\Delta G_{\mathrm{Elec}}(20)$, both $G_{\mathrm{Elec}}(19)$ and $G_{\mathrm{Elec}}(20)$ are calculated using eq 23, whereas to calculate $\Delta G_{\mathrm{Elec}}(21)$, both $G_{\mathrm{Elec}}(20)$ and $G_{\mathrm{Elec}}(21)$ are calculated using eq 29.

5. Simulation Details

The geometries of the Al_n ($n \leq 7$) clusters were optimized at the QCISD/6-31+G(d) level using the Gaussian 03 suite of programs.[40] Geometry optimization and vibrational frequency analysis for the Al_9, Al_{10}, and $\mathrm{Al}_{20}-\mathrm{Al}_{30}$ particles, TDDFT calculation for the Al_9 and Al_{10} clusters, and single-point PBE0/MEC calculations for the $\mathrm{Al}_{45}-\mathrm{Al}_{60}$ particles were performed using the NWCHEM 5.0 package.[42] Other DFT calculations were all done with Gaussian 03. Single-point CCSD(T)/aug-cc-pVnZ (n = D, T, Q) calculations were performed using the Molpro quantum chemistry package.[43]

For the MCCI calculations for $n = 2-4$, all of the runs were performed using the FPIMC code developed by Mielke at al.[21] (This path integral code performs the calculations classically in the present work because the Fourier expansion length K[21] is set to zero.) The parameters used for the MCCI calculation are listed in Table S5 of Supporting Information. To reduce the costs of the Monte Carlo sampling, the contributions from the points with short bond distances (<1.7 Å) and long bond distances (dissociated configurations, $> r_c$) are zeroed out. The mass of Al used is 26.98154 amu. The zero of the energy was taken as the global potential minimum of the molecule. Gaussian importance functions were used in the sampling. The Gaussians are functions of the Al−Al distance centered at the global minimum of the PES. The global minimum of Al_3 is an equilateral triangle while that of Al_4 is a tetrahedron for all of the potentials except NP-A-2347, for which it is a square. Therefore, the importance-function center parameters are always the shortest bond distance of Al−Al at the global minimum. The importance function width parameters were partially optimized in small initial trials. As in previous work,[44] the efficiency of the sampling did not improve much upon further optimization of these parameters.

In the MCEC calculations, systems consisting of 50 atoms in the canonical ensemble were simulated for the NP-A potential, and 100-atom systems were chosen for the less expensive NP-B potential. The biasing potentials were adjusted during the equilibration period such that each particle size between 1 and 10 is obtained with a nonnegligible probability for the NP-A potential using AVBMC-A, between 1 and 20 for the NP-B potential using AVBMC-A, and between 1 and 60 for the NP-B potential using AVBMC-L. For the NP-A potential, four independent simulations were performed for each temperature. For the NP-B potential, eight independent simulations were performed with AVBMC-A, and four were performed with AVBMC-L. For the NP-A potential, the equilibration period consists of 500 000 Monte Carlo cycles followed by 500 000 cycles for production runs. For the NP-B potential using AVBMC-A, the equilibration period consisted of 10^6 cycles, followed by 10^6 cycles of production runs. For AVBMC-L, both periods were extended to 3×10^6 cycles. During each production run, the biasing potential, as a function of the largest particle size, was fixed to that obtained at the end of the respective equilibration run.

6. Results and Discussion

6.1. Dimer Formation. The formation of the dimer will be discussed in more detail since accurate experimental results are available for the dimer formation. The comparison to our theoretical results can serve as a validation to the methods we used.

The standard Gibbs free energy change of reaction of $2\mathrm{Al} \rightarrow \mathrm{Al}_2$ can be calculated from the Gibbs free energies of formation of the monomer and the dimer. The free energy of formation of the monomer can be calculated from the ideal gas law, the electronic energy levels of the Al atom,[45] and the standard heat of vaporization.[8] Al_2, however, is more troublesome. Although the free energy of formation of Al_2 is available from the JANAF-NIST tables,[8,46] the experimental data used have several problems: (1) the experimental bond spectrum[47] it adopts is for the first electronic excited state ($^3\Sigma_g^-$) of Al_2, not the $^3\Pi_u$ ground state;[48,49] (2) the bonding energy of 1.56 eV[50] is also too high compared with the new experimental results of 1.34 eV[48] and other high level theoretical results (see also Table 1);[49] and (3) the electronic energy levels used are taken from those of B_2. We therefore repeat the thermodynamic calculations for Al_2. The reader is referred to Supporting Information for the

TABLE 1: Experimental and Theoretical Data Used to Calculate Al_2 Thermodynamic Functions

state	source	D_e (kcal mol^{-1})	T_0 (cm^{-1})	r_e (Å)	ω_e (cm^{-1})	$\omega_e x_e$ (cm^{-1})	B_e (cm^{-1})	α_e (cm^{-1})
$^3\Pi_u$	exp[48]	31.3 (30.9)[a]	0	2.7011	285.8	0.90	0.171	0.0008
	CMRCI[49]	33.5	0	2.7156	283.0	1.52	0.169	0.0013
	present[b]	32.7	NA	2.7013	NA	NA	NA	NA
$^3\Sigma_g^-$	exp[48]	30.9 (30.4)[a]	170	2.4665	350.0	2.02	0.205	0.0012
	CMRCI[49]	32.8	169	2.4840	349.0	2.05	0.202	0.0015
$^1\Sigma_g^+$	CMRCI[49]	26.8	2155	2.9617	227.2	1.07	0.142	NA
$^1\Pi_u$	CMRCI[49]	24.1	3130	2.7288	273.6	1.79	0.168	NA
$^1\Pi_g$	CMRCI[49]	23.6	3304	2.5328	316.6	2.41	0.195	NA

[a] Value in the parenthesis is D_0 value. [b] CCSD(T)/aug-cc-pV(n+d)Z//QCISD/6-31+G(d), [with n = D, T, Q] single-point energies exponentially extrapolated to complete basis set limit.

TABLE 2: Rovibrational Partition Functions[a] of Al_2

	NP-A		NP-B		NP-B-2347	
T (K)	DCI[b]	MCCI[c]	DCI[b]	MCCI[c]	DCI[b]	MCCI[c]
100	0.587	0.587	0.346	0.346	0.406	0.406
500	14.9	14.9	8.84	8.84	10.4	10.4
1100	74.2	44.2	44.2	44.2	52.4	52.4
1500	141	141	84.2	84.2	100	100
2100	285	286	172	172	206	207
2500	413	418	250	252	302	304
3100	648	677	400	408	484	498

[a] For tabulation, all values in this table have been divided by 100. The quantities in this table are all classical with the zero of energy at the minimum of the potential. [b] Numerically integration of configuration integrals using eq 9. [c] Monte Carlo integration of configuration integrals using eq 10.

equations[51] used for calculating thermodynamic functions and the full tables of the resulting thermodynamic properties.

The q_{Rov} of Al_2 calculated by different methods are listed in Table 2. Table 2 indicates that the agreement of DCI and MCCI is excellent. These results indicate that the MCCI method is indeed very accurate. We find that q_{Rov} calculated by the NP-B potential is smaller than those calculated by the NP-A potential, this is because NP-B gives a much deeper potential well, and thus at the NP-B level, Al_2 has sparser vibrational energy levels. Using the refitted NP-B-2347 potential, we find that calculated q_{Rov} are closer to those given by the NP-A potential, which is the analytic potential that provides the most accurate fit for the dimer.

$\Delta G°(2)$ calculated by different methods are listed in Table 3. For comparison, the experimental results calculated using a partition function of Al_2 calculated by either assuming the electronic partition function is nonseparable or assuming it is separable from rovibrational partition function; that is, the electronic excited state has the same q_{Rov} as the electronic ground state ($q_{Rov}^{(1)}$, where "1" denotes the ground state). Since DCI and MCCI give almost the same q_{Rov}, only free energy changes calculated by the DCI method are presented in Table 3. From Table 3, the separable approximation works well for Al_2, where the experimental results obtained without employing separable approximation are just slightly higher (0.5 kcal/mol at 3100 K) than the value calculated using $q_{Rov}^{(1)}$ for all states. Table 3 indicates that, without any correction terms, different potentials give very different results, where NP-A tends to give the smallest free energy changes, while NP-B gives the largest ones. After including all of the three correction terms, the three potentials give almost the same results. The maximum difference in the free energy changes is found at 3100 K for NP-A and NP-B-2347, whose difference is just 0.5 kcal/mol, whereas without the corrections, the difference is as high as 9 kcal/mol for NP-A and NP-B at 100 K.

After correction, the theoretical predictions are much closer to the experimental results. However, there is still a 5.3 kcal/mol difference at 3100 K between the NP-A result and the experiment. There are three causes for this difference. The first one is that the experimental D_e value for Al_2 is smaller than the present CC/CBS value by 1.4 kcal/mol. The second one comes from the difference in the electronic partition functions. In the present study using PBE0/MG3 method, we have optimized the geometry of Al_2 at each spin state and have calculated excitation energies by TDDFT method to get a well-converged electronic partition function. The electronic partition function is larger than that using the data in Table 1. In the last two columns of Table 3, the results using the present accurate D_e value (see Supporting Information, where the D_0 used is calculated from the present accurate theoretical D_e and experimental zero-point vibrational energy of the electronic ground state of Al_2), and the results (in the last column) using the present accurate D_e value as well as the electronic partition function at the TD-PBE0/MG3 level with a separable assumption are presented. Therefore, for the results in the last column, the only experimental data used are the bond spectrum of the electronic ground state. One can see that, using the present accurate D_e value, the free energy changes are lowered by 1.4 kcal/mol and, using the TD-PBE0/MG3 electronic partition function, they are further lowered, by about 1 kcal/mol. After these corrections, the experimental values differ by less than 0.7 kcal/mol from the corrected NP-A values (with smaller deviations found at lower temperatures). This agreement validates our method to calculate free energy changes.

6.2. Partition Functions of Al_3 and Al_4. The partition function of Al_3 and Al_4 are tabulated in Tables S6 and S7 of Supporting Information. Values of q_{IsoRov} calculated by the MCCI method using different potentials are very different, especially for Al_4, for which only NP-A-2347 correctly predicts a planar structure (D_{4h}) as the global minimum of Al_4. (It is well-established that the global minimum of the Al_4 clusters is a planar structure.[11,30−32,52−54]) We have proposed a method to improve the contribution of q_{IsoRov} to the free energy change by scaling q_{IsoRov} calculated with LL methods with a scaling factor given by eq 34. For small clusters, we are able to actually calculate q_{IsoRov} in a nonseparable way by the MCCI method with different potentials (both HL and LL) to verify that this strategy works. In Table 4, q_{IsoRov} calculated with the HL NP-A-2347 potential and the scaled values for the LL NP-B and NP-B-2347 potentials are given. For Al_3, f_{IsoRov}^{HLC} is between 2.6 and 2.7 for the NP-B potential and is 2.1 for the NP-B-2347 potential. For Al_4, f_{IsoRov}^{HLC} is between 3.4 and 5.5 and is between 3.9 and 6.7 for the NP-B and NP-B-2347 potentials, respectively. After scaling, q_{IsoRov} calculated by the LL methods are greatly improved and are very close to each other and much closer to those calculated by the HL method (Table 4), the exception being Al_4 at 100 K. It should be noted that although the relative error for q_{IsoRov} at 100 K is large, the error induced in the free energy change is small; for example, a factor of 5 only

TABLE 3: Standard Gibbs Free Energy Change (kcal/mol) of the $2Al \rightarrow Al_2$ Reaction Calculated by the DCI Method

	NP-A		NP-B		NP-B-2347					
T (K)	before[a]	after[b]	before[a]	after[b]	before[a]	after[b]	exp[c]	exp[d]	exp[e]	exp[f]
100	−34.2	−30.9	−43.2	−30.9	−38.6	−30.9	−29.4	−29.4	−30.9	−30.9
500	−27.3	−22.7	−35.9	−22.7	−31.5	−22.7	−21.0	−21.1	−22.4	−22.6
1100	−16.4	−9.9	−24.4	−9.9	−20.2	−9.9	−7.6	−7.9	−9.0	−9.7
1500	−9.0	−1.3	−16.5	−1.4	−12.5	−1.4	1.4	1.1	0.0	−1.1
2100	2.3	11.5	−4.7	11.4	−0.9	11.3	15.0	14.5	13.6	11.9
2500	9.9	20.0	3.2	19.9	6.9	19.8	24.0	23.5	22.6	20.6
3100	21.3	32.9	15.2	32.7	18.6	32.5	37.6	37.1	36.2	33.6

[a] No high-level correction is applied. [b] Corrected with eq 21. [c] Experimental results calculated using experimental data in Table 1 if available, otherwise using CMRCI results. [d] Experimental results calculated with separable partition functions given by eq 4, i.e., the rovibrational partition function of the electronic excited state is the same as the electronic ground state ($q_{\mathrm{Rov}}^{(1)}$). [e] Same as *c* but use the current value of 32.7 kcal/mol for the D_e of Al_2. [f] Same as *d* but q_{Elec} is calculated using energy levels given by the present TD-PBE0 calculations.

TABLE 4: Isomeric-Rovibrational Partition Functions of Al_3 and Al_4

	Al_3			Al_4		
T (K)	NP-A-2347	NP-B[a]	NP-B-2347[b]	NP-A-2347	NP-B[a]	NP-B-2347[b]
100	32.3	152	152	44.2	14.4	7.80
500	2.35×10^5	2.28×10^5	2.30×10^5	8.38×10^6	3.68×10^6	3.65×10^6
1100	9.55×10^6	9.08×10^6	9.39×10^6	4.91×10^9	2.41×10^9	2.41×10^9
1500	4.23×10^7	4.10×10^7	4.33×10^7	6.38×10^{10}	3.55×10^{10}	3.62×10^{10}
2100	2.18×10^8	2.23×10^8	2.38×10^8	1.12×10^{12}	6.63×10^{11}	7.19×10^{11}
2500	5.13×10^8	5.52×10^8	5.94×10^8	5.30×10^{12}	3.07×10^{12}	3.50×10^{12}
3100	1.48×10^9	1.72×10^9	1.87×10^9	4.08×10^{13}	2.20×10^{13}	2.73×10^{13}

[a] MCCI q_{IsoRov} scaled using eq 34 with NP-A-2347 as HL method and NP-B as LL method. [b] MCCI q_{IsoRov} scaled using eq 34 with NP-A-2347 as HL method and NP-B-2347 as LL method.

TABLE 5: Standard Gibbs Free Energy Change (kcal/mol) of R1 with $n = 2-4$, without High-Level Corrections

		MCCI	AVBMC-A	MCCI	AVBMC-A	AVBMC-L
T (K)	n	NP-A[a]	NP-A[a]	NP-B	NP-B[a]	NP-B[b]
1500	2	−9.0	−9.0	−16.5	−16.5	−16.5 + 0.8
1500	3	−12.7	−12.4	−17.9	−17.6	−17.6 + 0.2
1500	4	−20.3	−20.2	−20.4	−20.8	−21.0 + 0.1
2500	2	9.8	9.8	3.2	3.3	3.6 + 0.1
2500	3	7.7	8.1	3.7	3.7	3.6 + 0.3
2500	4	2.2	2.7	0.4	2.1	1.8 + 0.2

[a] Uncertainties (standard error of the mean computed from the independent simulations) are 0.1 kcal/mol. [b] Uncertainties (standard error of the mean computed from the independent simulations) are marked.

introduces an error of 0.3 kcal/mol in the free energy change at 100 K. For Al_4, the scaled q_{IsoRov} values are still just half of those of the high-level accurate values. Although a factor of 2 introduces an error of 4.1 kcal/mol in the free energy change at 3000 K, this is the best we can do to improve the results calculated by the less accurate potentials. In addition, the extent of the remaining error depends on *n*; thus, the situation for other particles is probably not as bad as that for Al_4 because, for Al_4, the global minimum optimized by the NP-A-2347 potential is very different from those optimized by the other three potentials, whereas for particles with $n > 5$, the global minima of Al_n particles are all nonplanar.[16,30−32]

6.3. $\Delta G°(n)$ of R1 with $n = 2-4$ without HLC. The standard Gibbs free energy changes of R1 with $n = 2-4$ calculated by the MCCI and MCEC methods with the NP-A and NP-B potentials are listed in Table 5. Except for $n = 4$ at 2500 K, for which the difference between the two methods is more than 1 kcal/mol for the NP-B potential, different methods with the same potential give almost the same results. This excellent agreement between two completely different approaches indicates that our methods to calculate the free energy change of R1 are very reliable.

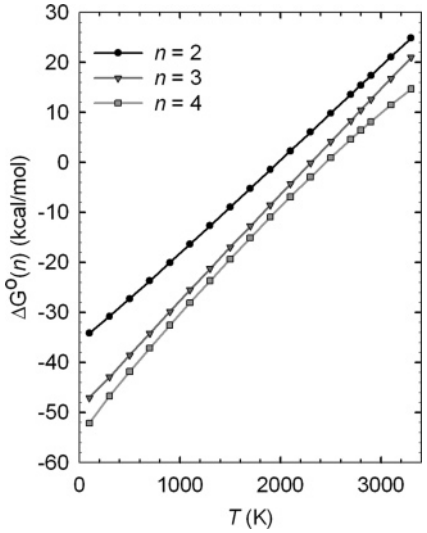

Figure 1. $\Delta G°(n)$ without HLC for the $Al + Al_{n-1} \rightarrow Al_n$ reaction ($n = 2$, 3, and 4) calculated by the MCCI method with the NP-A-2347 potential.

In Figure 1, $\Delta G°(n)$ calculated by the MCCI method for the NP-A-2347 potential is plotted as a function of temperature for $n = 2$, 3, and 4. For $n = 2$ and 3, the plotted curves are essentially linear, while for $n = 4$, there is curvature. This temperature dependence of $\Delta G°(n)$ can be rationalized by using the analytic expression of eq 2 in the classical limit. If a molecule has only one isomer, assuming that q_{Rov} is separable and neglecting q_{Elec}, eq 4 reduces to

$$Q(n) = q_{\mathrm{Trans}} q_{\mathrm{Vib}} q_{\mathrm{Rot}} \tag{36}$$

If the classical expression (eq 33) for q_{Vib} is used, it is easy to show that

$$\Delta G°(n) = \Delta E_e + RT(D - l \ln T) \tag{37}$$

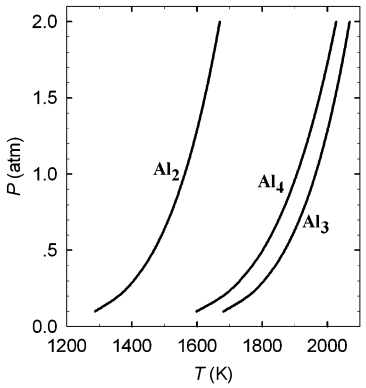

Figure 2. Coexistence "phase" diagram of Al, Al_2, Al_3, and Al_4 obtained using $\Delta G°(n)$ values with full corrections.

where D and l are constants (details of the derivation are given in Supporting Information). Interestingly, this analysis indicates that for $n = 2$, l is negative, for $n = 3$, l is zero, and for $n > 3$, l is positive. The curvatures of the three lines agree very well with this prediction. Therefore, eq 37 can be used to predict $\Delta G°(n)$ for those temperatures for which $\Delta G°(n)$ have not been directly simulated. In addition, this analytic form can be used to predict the temperature at which $\Delta G°(n)$ is equal to zero. Applying the ideal gas law, the pressure dependence of $\Delta G(n)$ can be shown to be

$$\Delta G(n,P,T) = \Delta G°(n) - RT \ln(P/P°) \qquad (38)$$

where $P°$ is the standard pressure, which is 1 atm in the present study. Therefore, it is possible to predict a "phase diagram" for Al_n particle formation. Figure 2 shows such diagrams for Al_2, Al_3, and Al_4, where the $\Delta G°(n)$ values used to compute the figure are given by the MCCI method with all three HLC terms included.

6.4. $\Delta G°(n)$ for Forming Larger Particles Calculated by the MCEC Methods. In the previous two sections, $\Delta G°(n)$ values with $n = 2-4$ given by several completely different approaches are in excellent agreement with each other. This validates our methods of calculating $\Delta G°(n)$. However, the MCCI method, although accurate, is expensive for large molecules. On the other hand, the MCEC methods can be applied to much larger particles, and it has the advantage of simulating all of the equilibrium constants of R1 with $n \leq N$ (number of Al atoms in the simulation box) at a given temperature in one single simulation. Here, we present the results obtained by the MCEC methods.

Equation 14 indicates that, for a large enough simulation cell volume, V, the error in $\Delta G°$ for dimer formation due to a finite N in the simulations is $RT \ln(1 - 1/N)$. Thus, with $N = 50$, the error in $\Delta G°$ is 0.02 RT and is 0.01 RT for $N = 100$. Figure 3 shows $\Delta G°$ as a function of the number of particles, N, in canonical ensemble simulations at 2800 K. The solid line is the result obtained from eq 14, which is asymptotically correct in the limit of large volume. The squares denote the results from canonical ensemble simulations. Clearly, the volume of the simulation cell is large enough to reproduce the correct results. In view of Figure 3, we choose $N = 100$ for the less expensive NP-B potential and $N = 50$ for the NP-A potential. Consequently, for each temperature, the simulation volume is chosen large enough such that the correct $\Delta G°$ for the dimer formation is reproduced.

Figure 4 shows $\Delta G°(n)$ as a function of n for 1500 and 3000 K. For each temperature, AVBMC-A and AVBMC-L give essentially the same value for $\Delta G°(n)$ if the same potential is used, as expected. Accordingly, in the discussion below, we do not differentiate between the two methods for NP-B. (For AVBMC-L and $n < 30$, the large scatter at the higher temperatures is due to the larger uncertainties resulting from our emphasis on using this method to calculate the larger particles more accurately because they could not be sampled

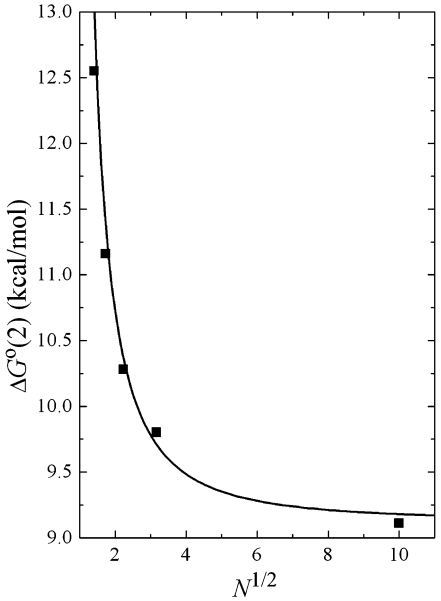

Figure 3. $\Delta G°(2)$ (with $n = 2$ in R1) at 2800 K with the NP-B potential as a function of $N^{1/2}$, where N is the number of particles in the simulation cell. The solid line is eq 14, and the squares are from simulations.

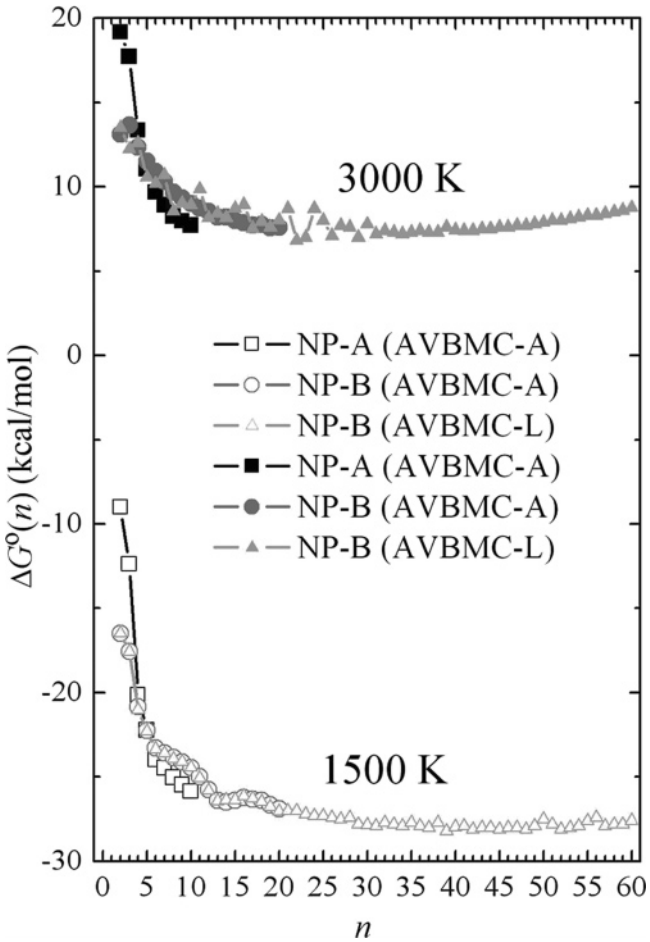

Figure 4. $\Delta G°(n)$ of R1 given by the MCEC methods without HLC as a function of n at 1500 and 3000 K.

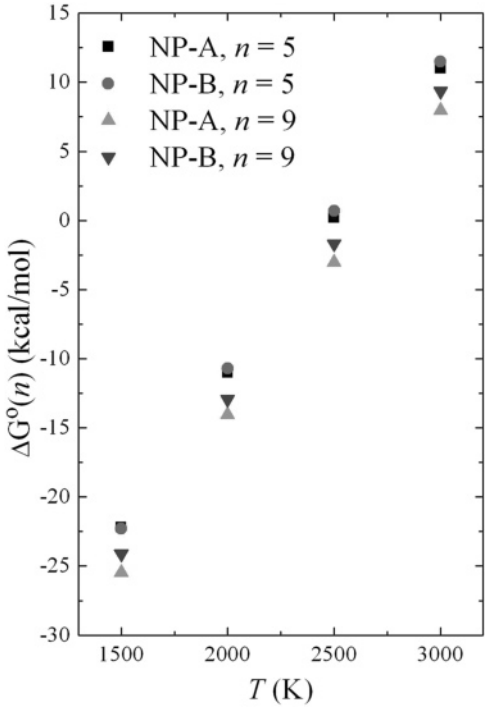

Figure 5. $\Delta G°(n)$ of R1 given by the AVBMC-A method without HLC as a function of temperature for $n = 5$ and $n = 9$.

well with AVBMC-A, which did quite well for the smaller particles.) At 1500 K, $\Delta G°(n)$ (with a standard state of 1 atm) is negative, indicating that the particle form is more favorable at 1 atm. On the other hand, $\Delta G°(n)$ is positive at 3000 K, reflecting that at this temperature the gaseous state is more stable. For large values of n, a bulk-like behavior is expected with a constant $\Delta G°(n)$; however, the cluster sizes involved here are not large enough to observe that, especially at 3000 K.

Another feature that emerges from Figure 4 is that $\Delta G°(n)$ seemingly approaches a unique plateau value for each temperature. This can be understood by referring to the definition of $\Delta G°(n)$ for each particle size: $\Delta G°(n) = G°(n) - [G°(n-1) + G°(1)]$. In the limit of large n, interfacial effects become negligible; the resulting "nanoparticle" has, essentially, homogeneous bulk properties, and the free energy becomes an extensive thermodynamic variable. Consequently, $G°(n) - G°(n-1)$ approaches a constant value, the chemical potential of a bulk aluminum atom. Despite this expected behavior, we do not assume that $\Delta G°(60)$ values can be associated with a macroscopically large particle because $n = 60$ is not large enough to reach the bulk limit. For a macroscopic particle, that is, when $n \rightarrow \infty$, at temperatures where an aggregated state is the most stable form, $-\Delta G°(n)$ is the standard Gibbs free energy of formation of gaseous Al, which is 33.4 kcal/mol at 1500 K. In comparison, $-\Delta G°(60)$ at 1500 K is 27.6 kcal/mol. After applying all corrections, $-\Delta G°(60)$, however, is further away from the corresponding macroscopic value (see below).

$\Delta G°(n)$ for the reactions with different n can be studied as a function of temperature. Figure 5 shows such a plot for $n = 5$ and $n = 9$. For both of these reactions (as well as for all of the other cases not shown in Figure 5), $\Delta G°(n)$ is a monotonically increasing function of T. Such a trend is qualitatively similar to that obtained for a harmonic oscillator (eq 37). Figure 6 shows $\Delta G°(n)/RT$ as a function of T for the same reactions as in Figure 5. From the thermodynamic relation $d(\Delta G°(n)/RT)/dT = \Delta H°(n)/RT^2$ (where $\Delta H°(n)$ is the standard heat of reaction), Figure 6 shows that the standard heat of reaction is negative, which is consistent with the reactions in R1 being exothermic.

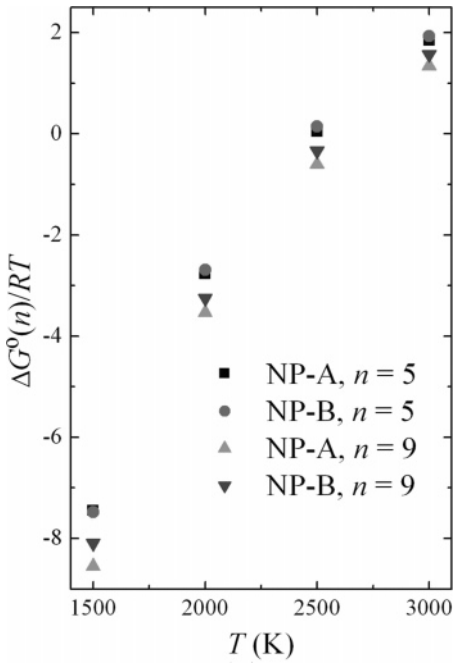

Figure 6. $\Delta G°(n)/RT$ of the reaction in R1 as a function of temperature for $n = 5$ and $n = 9$. $\Delta G°(n)$ is calculated by the AVBMC-A method without HLC.

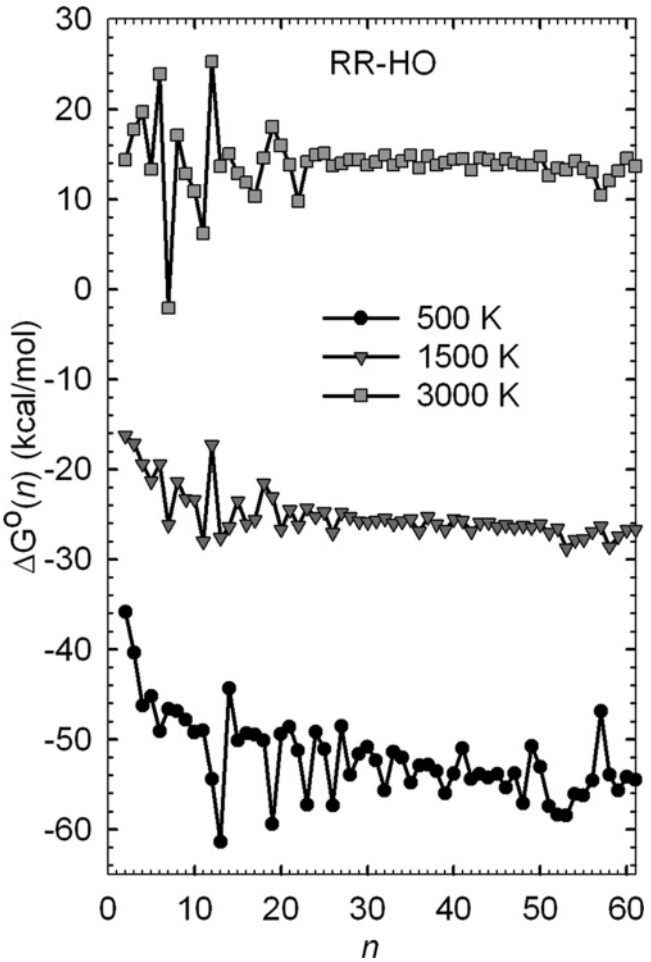

Figure 7. $\Delta G°(n)$ of R1 without HLC predicted by the RR-HO approximation.

It is interesting to compare the results obtained by the MCEC methods to those obtained with the RR-HO approximation. In Figure 7, $\Delta G°(n)$ obtained with the RR-HO approximation using

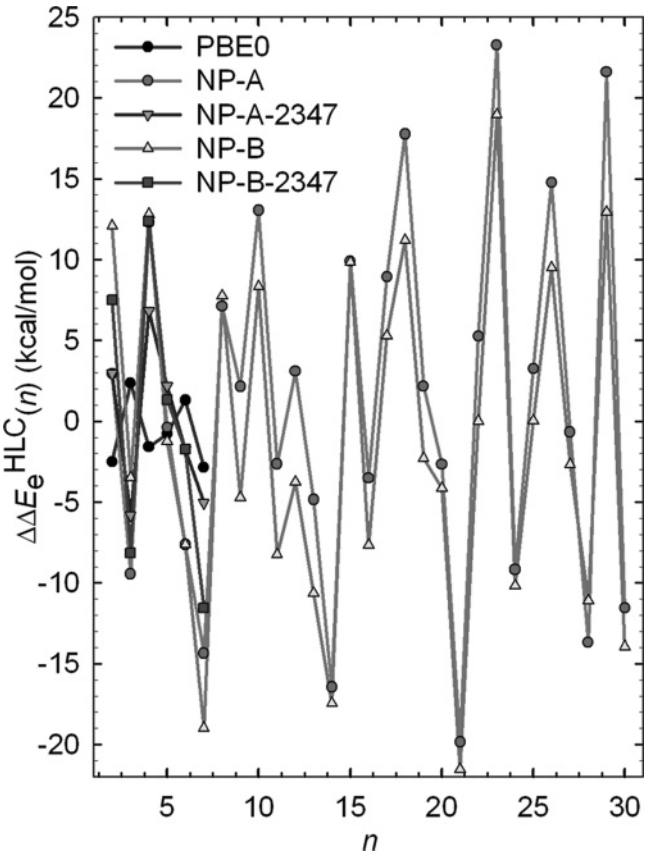

Figure 8. High-level correction to the potential energy difference of R1, i.e. $\Delta\Delta E_e^{HLC}(n)$, using the most accurate method available for each size as the HL method, as a function of particle size.

the NP-B potential is plotted as a function of size for 500, 1500, and 3000 K. Generally, the RR-HO approximation gives higher $\Delta G°(n)$ values, which means that the RR-HO approximation underestimates the partition function of the larger particles. At 500 K, the curve shows strong oscillations in the whole size range, where the wells can be identified as relatively stable particles (magic particles).[16] At 1500 and 3000 K, the oscillation becomes weaker for large n, in accordance with the accurate MCEC results. For small n, the oscillation is still strong, especially at 3000 K. It is expected that for small particles, one or two low-vibrational frequencies in different isomers may greatly affect the results (as mentioned before, a factor of 2 in the partition function brings about 4 kcal/mol change in free energy), since, at high temperatures, high-energy isomers may contribute most to the properties of the particle.[16] For the large particles, hundreds or even thousands of isomers make contributions;[16] thus, the contribution of several low-vibrational frequencies of an isomer is small after weighted by the Boltzmann factor ($e^{-\beta E_\gamma}$).

6.5. High-Level Correction to $\Delta E_e(n)$. First, we check the performance of different levels of theory for calculating the potential energy difference ($\Delta E_e(n)$) of reaction R1. We have optimized the geometries of the Al_n particles with $n = 2-30$ by the PBE0 method, and thus, we have accurate $\Delta E_e(n)$ values for comparison. In Figure 8, $\Delta\Delta E_e^{HLC}(n)$, that is, the error of different methods in calculating $\Delta E_e(n)$ using the most accurate method available for each n as the HL method, is plotted as a function of size, where the HL method is the CC/CBS method for $n = 2-7$ and is PBE0 for other n.

Figure 8 indicates that the PBE0/MG3 method is very accurate in calculating $\Delta E_e(n)$, as previously observed.[11] The mean absolute value of $\Delta\Delta E_e^{HLC}(n)$, that is, the mean unsigned error (MUE) in calculating $\Delta E_e(n)$ by the PBE0/MG3 method for the 6 clusters, is just 1.9 kcal/mol. For the analytic potentials, the MUEs are 7.8, 4.1, 9.4, and 7.1 kcal/mol, for the NP-A, NP-A-2347, NP-B, and NP-B-2347 potentials, respectively, for the particles with $n = 2-7$. Refitting of the NP-A and NP-B potentials greatly reduces the error in calculating $\Delta E_e(n)$. For the NP-A and NP-B potentials, for particles with $n = 2-30$, the errors are very large for some particles, more than 20 kcal/mol. The analytic potentials were fitted to minimize the error in calculating energies and the energy differences between different geometries of the same size,[7,10] and NP-A does perform better than NP-B on calculating cohesive energies (atomization energy per atom, see Figure 9). Therefore, it is expected that NP-A may perform better than NP-B in calculating the energy differences between different isomers of a given n, and thus may perform better in calculating its q_{IsoRov}.

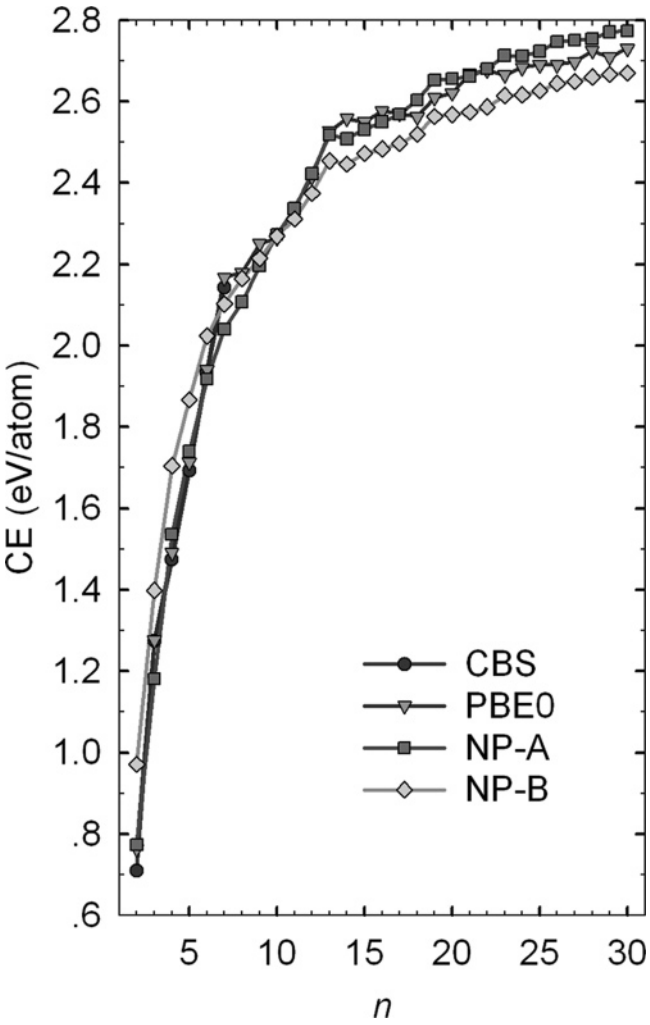

Figure 9. Cohesive energy of the Al_n particle with $n = 2-30$.

Final $\Delta\Delta E_e^{HLC}(n)$ for the whole range of n are listed in Table 6, where LL methods are NP-A-2347, NP-A, and NP-B for $n = 2-4$, $n = 5-10$, and $n = 11-60$, respectively, and HL methods are CC/CBS and PBE0 for $n = 2-7$ and $n = 8-60$, respectively.

6.6. Electronic Excitation Contributions. The density of electronic states reaches 10^3 eV^{-1} at ~4 eV for Al_{10} and between 2 and 3 eV for Al_{20}, but kT is only 0.26 eV at 3000 K, so the electronic partition functions are dominated by lower energies where the density of states is much sparser. For example, for Al_{20}, the electronic partition function is converged to 2% by 2 eV and to 24% by 1 eV, and convergence is faster for $n < 20$.

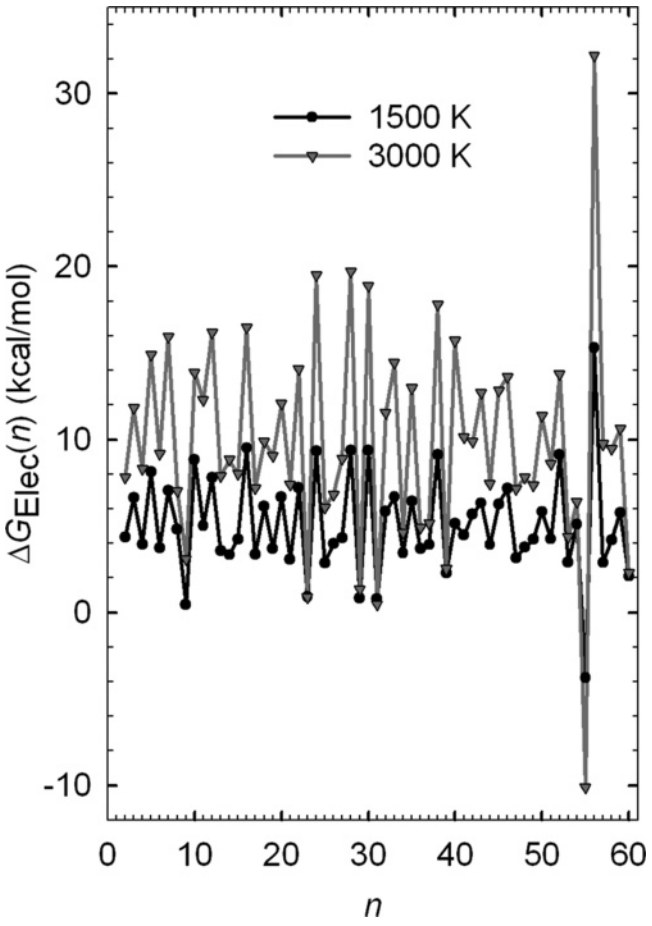

Figure 10. Electronic excitation contributions to $\Delta G°(n)$ of R1 at 1500 and 3000 K.

TABLE 6: High-Level Correction (kcal/mol) to the Potential Energy Change of R1

n	$\Delta\Delta E_e^{HLC}(n)$	n	$\Delta\Delta E_e^{HLC}(n)$	n	$\Delta\Delta E_e^{HLC}(n)$	n	$\Delta\Delta E_e^{HLC}(n)$
2	3.0	17	5.3	32	3.5	47	−2.4
3	−5.8	18	11.2	33	−1.1	48	−0.8
4	6.8	19	−2.3	34	−2.0	49	24.4
5	−0.4	20	−4.2	35	−13.0	50	−10.2
6	−7.6	21	−21.5	36	16.8	51	−3.7
7	−14.4	22	0.0	37	2.2	52	26.8
8	7.1	23	19.0	38	−9.0	53	14.8
9	2.2	24	−10.2	39	1.7	54	26.4
10	13.1	25	0.0	40	15.8	55	42.6
11	−8.2	26	9.5	41	−11.0	56	−39.4
12	−3.8	27	−2.7	42	10.5	57	−38.3
13	−10.7	28	−11.1	43	−1.2	58	0.4
14	−17.4	29	12.9	44	−11.8	59	2.4
15	9.9	30	−13.9	45	−6.5	60	10.2
16	−7.7	31	3.6	46	−4.6		

The electronic excitation contributions to the free energy change of R1, that is, the $\Delta G_{Elec}(n)$ values, are plotted as a function of particle size for 1500 and 3000 K in Figure 10. The plots show strong oscillations with particle size. Most $\Delta G_{Elec}(n)$ values are positive because the electronic partition function of the Al atom is large because of the small excitation energy from the ground electronic state ($^2P_{1/2}$) to the first electronic state ($^2P_{3/2}$), which is just 112 cm^{-1} (0.014 eV).[45] Thus, the major contribution to $\Delta G_{Elec}(n)$ is from the Al atom, which is a positive 10.5 kcal/mol at 3000 K, and one can see that, at 3000 K, $\Delta G_{Elec}(n)$ does oscillate around 10 kcal/mol. For some n, $\Delta G_{Elec}(n)$ is very large, for example, more than 30 kcal/mol for $n = 56$.

The final $\Delta G_{Elec}(n)$ values for 1500, 2000, 2500, and 3000 K are summarized in Table 7, and the electronic partition functions are tabulated in Supporting Information.

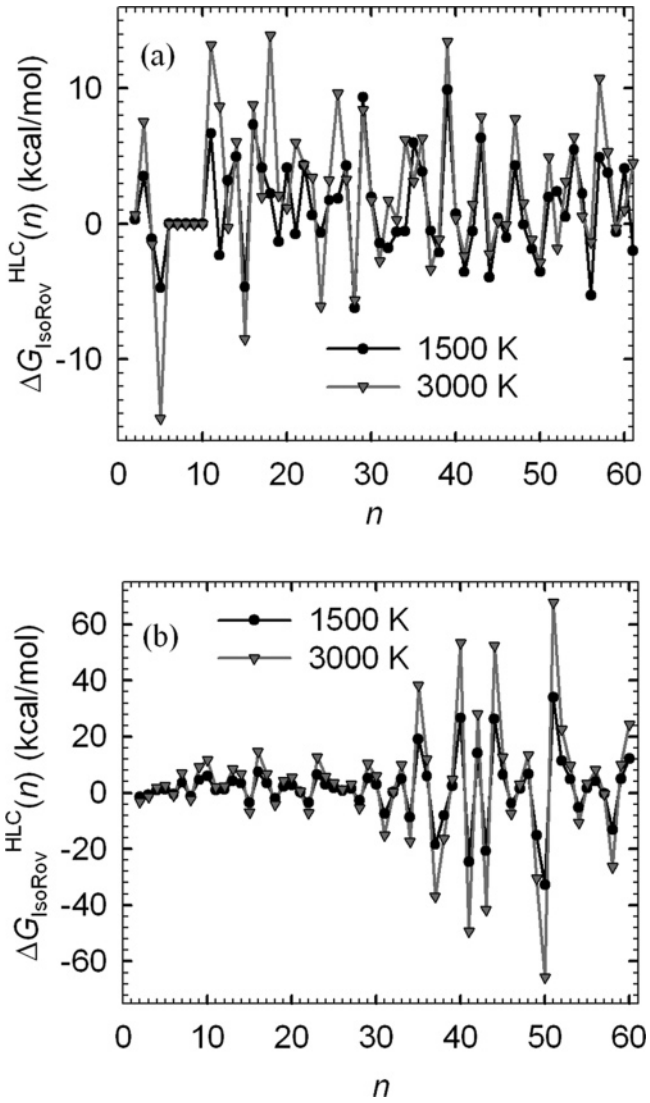

Figure 11. (a) Final $\Delta G_{IsoRov}^{HLC}(n)$ and (b) $\Delta G_{IsoRov}^{HLC}(n)$ calculated using only global minima with HL method as NP-A and LL method as NP-B.

6.7. Correction to the Isomeric−Rovibrational Partition Function. In Section 6.2., we have validated our method of correcting isomeric−rovibrational partition function using a scaling factor as defined by eq 34. Small particles with $n = 2-5$ have just a few low-energy isomers, and it is possible to optimize the geometries of these isomers and calculate their vibrational frequencies with the accurate PBE0/MG3 method. In the present study, we have optimized the geometries of two low-energy isomers for Al_3 (triangle and linear), two for Al_4 (tetrahedron and rhombus), and four for Al_5 (planar $C2_v$ structure, trigonal bipyramid, Jahn−Teller distorted pyramid (C_s), and a C_{2v} structure obtained by adding an Al atom to one edge of the tetrahedral Al_4). For the larger particles with $n = 6-30$, it is too expensive to explore all of the low-energy isomers with the DFT method; therefore, geometry optimization and frequency analysis were only performed for our best estimate of the global minimum structure of each n at the DFT level. However, it is dangerous to calculate $\Delta G_{IsoRov}^{HLC}(n)$ given by eq 35 using just the geometries and frequencies of global minima to calculate $f_{IsoRov}^{HLC}(n)$, since the properties of most particles at high temperatures cannot be represented by the global minimum.[16] Therefore, eq 35 is only applied to $n = 2-5$, where the HL method is PBE0/MG3 and the LL method is NP-

TABLE 7: Electronic Excitation Contribution ($\Delta G_{Elec}(n)$, kcal/mol) to the Standard Gibbs Free Energy Change of R1

T (K)\n	2	3	4	5	6	7	8	9	10	11	12	13	14	15
1500	4.3	6.6	4.0	8.1	3.7	7.0	4.8	0.5	8.9	5.0	7.8	3.6	3.3	4.2
2000	5.6	8.5	5.4	10.8	5.4	9.9	5.6	1.1	10.8	7.5	10.6	5.0	5.0	5.6
2500	6.7	10.2	6.9	13.0	7.2	12.9	6.3	1.9	12.5	9.9	13.4	6.4	6.8	6.9
3000	7.8	11.8	8.3	14.9	9.2	15.9	7.0	3.1	13.9	12.3	16.2	7.9	8.8	8.0

T (K)\n	16	17	18	19	20	21	22	23	24	25	26	27	28	29	30
1500	9.5	3.4	6.1	3.7	6.7	3.1	7.2	0.9	9.3	2.9	4.0	4.3	9.4	0.8	9.4
2000	12.1	4.7	7.5	5.4	8.6	4.4	9.7	0.9	12.8	4.1	4.9	5.9	12.8	1.1	12.5
2500	14.4	6.0	8.7	7.2	10.4	5.9	12.0	0.9	16.2	5.1	5.9	7.4	16.2	1.3	15.7
3000	16.5	7.2	9.9	9.1	12.1	7.4	14.1	0.9	19.5	6.1	6.8	8.9	19.7	1.3	18.9

T (K)\n	31	32	33	34	35	36	37	38	39	40	41	42	43	44	45
1500	0.8	5.8	6.7	3.5	6.4	3.7	3.9	9.1	2.3	5.2	4.5	5.7	6.3	3.9	6.3
2000	0.8	7.8	9.3	4.1	8.7	4.6	4.6	12.1	2.4	8.3	6.3	7.2	8.5	5.2	8.4
2500	0.7	9.6	12.0	4.3	10.9	5.0	4.9	15.0	2.5	12.0	8.2	8.6	10.6	6.5	10.5
3000	0.5	11.6	14.4	4.6	13.0	4.9	5.2	17.8	2.5	15.7	10.1	9.9	12.7	7.5	12.8

T (K)\n	46	47	48	49	50	51	52	53	54	55	56	57	58	59	60
1500	7.2	3.2	3.8	4.2	5.8	4.3	9.1	2.9	5.1	−3.8	15.3	2.9	4.2	5.8	2.1
2000	9.5	4.5	5.0	5.4	7.7	5.7	11.6	3.5	5.7	−6.1	21.6	4.4	6.0	7.4	2.4
2500	11.7	5.8	6.4	6.5	9.5	7.3	12.9	4.1	6.6	−8.9	27.4	6.7	7.7	8.9	2.1
3000	13.6	7.2	7.8	7.3	11.4	8.6	13.8	4.4	6.4	−10.1	32.2	9.7	9.5	10.6	2.3

TABLE 8: High-Level Correction for the Isomeric-Rovibrational Partition Function Contribution ($\Delta G^{HLC}_{IsoRov}(n)$, kcal/mol) to the Standard Gibbs Free Energy Change of R1

T (K)\n	2	3	4	5	6	7	8	9	10	11	12	13	14	15
1500	0.3	3.5	−1.1	−4.7	-	-	-	-	-	6.7	−2.3	3.2	5.0	−4.7
2000	0.4	4.8	−1.2	−7.4	-	-	-	-	-	9.1	1.9	3.3	3.5	−6.7
2500	0.5	6.1	−1.3	−10.7	-	-	-	-	-	11.3	6.0	1.3	4.5	−8.1
3000	0.6	7.5	−1.5	−14.4	-	-	-	-	-	13.2	8.7	−0.3	6.0	−8.5

T (K)\n	16	17	18	19	20	21	22	23	24	25	26	27	28	29	30
1500	7.3	4.1	2.2	−1.3	4.1	−0.7	4.3	0.6	−0.6	1.7	1.9	4.3	−6.2	9.4	2.0
2000	9.0	2.9	7.6	−0.1	2.0	0.9	5.2	1.7	−2.6	2.2	4.7	3.3	−6.5	9.8	2.1
2500	9.4	2.1	11.3	0.9	1.3	3.5	5.0	2.5	−4.4	2.8	7.3	2.9	−6.1	9.3	1.9
3000	8.8	2.0	13.9	2.1	1.2	6.0	4.3	3.4	−6.1	3.2	9.6	3.3	−5.6	8.4	1.7

T (K)\n	31	32	33	34	35	36	37	38	39	40	41	42	43	44	45
1500	−1.4	−1.8	−0.6	−0.5	6.0	3.8	−0.5	−2.1	9.9	0.8	−3.6	−0.6	6.4	−4.0	0.4
2000	−2.5	−0.6	−0.5	1.6	5.0	4.7	−1.5	−1.9	11.2	1.0	−3.4	0.0	7.0	−3.5	0.3
2500	−2.8	0.6	−0.1	3.8	4.0	5.5	−2.4	−1.5	12.4	0.8	−2.9	0.7	7.5	−3.0	0.3
3000	−2.8	1.7	0.3	6.2	3.1	6.3	−3.4	−1.1	13.5	0.4	−2.4	1.4	7.9	−2.2	0.2

T (K)\n	46	47	48	49	50	51	52	53	54	55	56	57	58	59	60
1500	−1.0	4.3	−0.1	−1.9	−3.6	2.0	2.4	0.5	5.5	2.2	−5.3	4.9	3.8	−0.6	4.1
2000	−0.6	5.4	0.3	−1.4	−3.4	2.9	1.0	1.1	5.5	1.5	−4.3	8.0	4.3	−0.7	3.0
2500	−0.3	6.6	0.8	−1.2	−3.1	3.9	−0.5	2.0	5.9	1.0	−2.8	9.7	4.8	−0.6	1.9
3000	−0.1	7.7	1.5	−1.2	−2.9	4.9	−1.8	3.1	6.4	0.6	−1.3	10.7	5.3	−0.3	1.0

A-2347 for $n = 2-4$ and is NP-A for $n = 5$ and is applied to $n = 11-60$, where the HL method is NP-A and the LL method is NP-B.

In Figure 11a, the final $\Delta G^{HLC}_{IsoRov}(n)$ is plotted as a function of particle size. For comparison, for $n = 2-60$, $\Delta G^{HLC}_{IsoRov}(n)$ values calculated using only global minima with NP-A as the HL method and NP-B as the LL method are plotted as a function of particle size in Figure 11b. It should be noted that for $n = 6-10$, no $\Delta G^{HLC}_{IsoRov}(n)$ is applied. The figure indicates that, if only global-minima geometries and frequencies are used, the corrections are much larger than those calculated with all isomers, especially for large n. This is in agreement with the finding that, for many large particles, the global minimum becomes less important and cannot represent the properties of the particle.[16]

The final $\Delta G^{HLC}_{IsoRov}(n)$ values for 1500, 2000, 2500, and 3000 K are summarized in Table 8.

6.8. Accurate Standard Gibbs Free Energy Change and Standard Gibbs Free Energy of Formation. A summary of the methods used for different ranges of n are listed in Table 9, where for $n \leq 10$ the simulation results are expected to have higher accuracy. Further improvement is possible, for example, to optimize the geometries of the global minimum for each particle using high-level methods or to calculate excitation energies for each particle.

Appling all of the correction terms, the final accurate standard Gibbs free energy changes ($\Delta G^{\circ}_{Acc}(n)$) are plotted as a function of size for 1500, 2000, 2500, and 3000 K in Figure 12. The final free energy changes are tabulated in Table 10. One σ statistical error bars of the free energy changes are available in Supporting Information. $\Delta G^{\circ}_{Acc}(n)$ show strong oscillation with cluster size. This oscillation is caused by the three high-level corrections while the uncorrected results show weak oscillation (Figure 4).

With these Gibbs free energy changes, the standard Gibbs free energy of formations can be obtained. There are two methods to obtain such values. The first one uses experimental

TABLE 9: Methods Used for the Accurate Standard Gibbs Free Energy Change ($\Delta G°(n)$) of R1

	$\Delta G°(n)$		$\Delta\Delta E_e^{HLC}(n)$		$\Delta G_{Elec}(n)$		$\Delta G_{IsoRov}^{HLC}(n)$	
n	method	potential	HL	LL	HL	$G_{Elec}(n)$	HL	LL
2−4	MCCI	NP-A-2347	CC/CBS[a]	NP-A-2347	PBE0/MG3	eq 23	PBE0/MG3	NP-A-2347
5	AVBMC-A	NP-A	CC/CBS[a]	NP-A	PBE0/MG3	eq 23	PBE0/MG3	NP-A
6−7	AVBMC-A	NP-A	CC/CBS[a]	NP-A	PBE0/MG3	eq 23	none	none
8−10	AVBMC-A	NP-A	PBE0/MG3	NP-A	PBE0/MG3	eq 23	none	none
11−13	AVBMC-A	NP-B	PBE0/MG3	NP-B	PBE0/MEC	eq 23	NP-A	NP-B
14−20	AVBMC-A	NP-B	PBE0/MEC	NP-B	PBE0/MEC	eq 23	NP-A	NP-B
21−30	AVBMC-L	NP-B	PBE0/MEC	NP-B	PBE0/MEC	eq 23	NP-A	NP-B
31−60	AVBMC-L	NP-B	PBE0/MEC//NP-A[b]	NP-B	PBE0/MEC//NP-A[b]	eq 29	NP-A	NP-B

[a] CCSD(T)/aug-cc-pV(n+d)Z//QCISD/6-31+G(d), [with n = D, T, Q] single-point energies exponentially extrapolated to complete basis set limit. [b] Single-point energies on NP-A global minimum geometries, which are obtained by reoptimizing all NP-B located low-energy isomers (2000 at most).

TABLE 10: Final Standard Gibbs Free Energy Change ($\Delta G°(n)$, kcal/mol) of R1

T (K)\n	2	3	4	5	6	7	8	9	10	11	12	13	14	15
1500	−1.3	−12.7	−9.7	−19.2	−27.9	−31.8	−13.1	−22.9	−3.9	−21.6	−24.0	−30.3	−35.6	−17.0
2000	9.3	1.0	2.2	−8.0	−14.6	−17.6	−0.9	−10.8	9.5	−5.3	−5.3	−16.5	−23.5	−5.8
2500	20.0	14.6	13.3	2.2	−1.6	−3.4	10.7	1.1	22.3	10.7	13.0	−5.8	−9.1	5.4
3000	30.6	28.2	23.4	11.2	11.2	10.5	22.4	13.2	34.6	25.9	29.6	5.2	5.6	17.3

T (K)\n	16	17	18	19	20	21	22	23	24	25	26	27	28	29	30
1500	−17.0	−13.6	−6.8	−26.6	−20.2	−46.2	−15.4	−6.7	−28.8	−22.7	−12.1	−21.6	−35.4	−4.7	−30.4
2000	−1.2	−2.0	11.3	−12.1	−8.7	−31.4	−0.2	6.2	−15.3	−9.4	3.4	−9.4	−20.4	8.3	−15.2
2500	12.7	10.0	27.6	2.1	3.7	−16.1	13.5	18.2	−2.1	3.9	18.3	3.5	−4.9	19.3	−0.5
3000	25.5	22.2	42.7	16.4	16.7	0.6	25.2	30.3	11.9	17.3	33.0	17.2	10.6	29.7	14.5

T (K)\n	31	32	33	34	35	36	37	38	39	40	41	42	43	44	45
1500	−24.9	−20.2	−22.8	−27.0	−28.2	−3.6	−22.4	−29.7	−14.3	−6.3	−38.0	−12.5	−16.5	−39.8	−28.0
2000	−13.9	−4.9	−8.2	−12.1	−15.0	10.0	−10.6	−14.6	−0.6	9.2	−24.0	1.8	−1.5	−25.9	−13.6
2500	−2.7	9.5	6.4	1.8	−2.2	23.1	0.5	0.3	12.3	24.4	−9.8	15.7	12.8	−12.3	0.3
3000	8.5	24.1	20.9	16.0	10.4	35.4	11.3	15.0	25.3	39.3	4.2	29.2	26.9	0.9	14.1

T (K)\n	46	47	48	49	50	51	52	53	54	55	56	57	58	59	60
1500	−26.5	−23.0	−25.2	−1.1	−35.4	−25.3	10.2	−9.8	9.1	13.5	−56.7	−58.4	−19.5	−20.2	−11.2
2000	−11.5	−8.2	−11.4	12.8	−21.5	−10.8	23.8	3.7	22.1	22.5	−37.4	−41.3	−4.7	−6.2	0.3
2500	2.7	6.1	2.4	25.9	−7.6	3.8	35.5	17.2	35.4	31.2	−18.2	−25.2	9.5	7.6	11.2
3000	16.5	20.2	16.2	38.4	6.2	17.8	46.7	30.3	47.4	41.3	−0.2	−9.4	23.6	21.3	22.2

TABLE 11: Standard Gibbs Free Energy of Formation (kcal/mol) of Al_n (n = 1−60) Particles

T (K)\n	1[a]	2[b]	3	4	5	6	7	8	9	10	11	12	13	14	15
1500	33.4	68.3	89.1	112.8	127.1	132.7	134.3	154.6	165.2	194.7	206.6	216.0	219.2	217.0	233.5
2000	20.2	53.2	74.4	96.8	109.1	114.7	117.3	136.7	146.1	175.8	190.8	205.8	209.5	206.2	220.6
2500	7.4	38.8	60.7	81.4	90.9	96.7	100.7	118.7	127.2	156.8	174.8	195.2	196.8	195.1	207.8
3000	0.0	35.4	63.6	87.0	98.2	109.4	119.9	142.2	155.4	190.1	216.0	245.6	250.8	256.4	273.7

T (K)\n	16	17	18	19	20	21	22	23	24	25	26	27	28	29	30
1500	249.9	269.8	296.4	303.2	316.4	303.7	321.7	348.4	353.1	363.8	385.2	397.1	395.2	423.9	426.9
2000	239.6	257.9	289.4	297.5	309.0	297.8	317.9	344.3	349.2	360.1	383.7	394.5	394.4	422.9	428.0
2500	227.9	245.2	280.2	289.7	300.8	292.0	312.8	338.4	343.7	354.9	380.6	391.4	393.8	420.5	427.3
3000	299.2	321.4	364.2	380.5	397.3	397.8	423.0	453.3	465.3	482.6	515.6	532.8	543.4	573.0	587.5

T (K)\n	31	32	33	34	35	36	37	38	39	40	41	42	43	44	45
1500	435.4	448.7	459.3	465.8	471.0	500.8	511.9	515.6	534.7	561.9	557.4	578.4	595.3	588.9	594.4
2000	434.3	449.6	461.6	469.8	475.0	505.2	514.9	520.5	540.1	569.6	565.9	587.9	606.6	600.9	607.6
2500	432.0	448.8	462.6	471.8	476.9	507.4	515.2	522.9	542.6	574.3	571.9	594.9	615.1	610.1	617.7
3000	596.0	620.1	641.0	657.0	667.4	702.8	714.1	729.1	754.4	793.7	797.8	827.0	853.9	854.8	868.9

T (K)\n	46	47	48	49	50	51	52	53	54	55	56	57	58	59	60
1500	601.4	611.8	620.1	652.4	650.4	658.5	702.1	725.7	768.3	815.2	791.9	766.9	781.4	794.1	816.4
2000	616.3	628.3	637.2	670.2	668.9	678.4	722.4	746.4	788.7	831.4	814.2	793.2	809.2	822.8	843.3
2500	627.8	641.2	651.0	684.3	684.0	695.2	738.1	762.7	805.5	844.0	833.2	815.4	832.8	847.2	865.8
3000	885.4	905.6	921.8	960.2	966.4	984.1	1030.9	1061.2	1108.6	1150.0	1149.7	1140.4	1164.5	1185.3	1207.5

[a] Experimental values from ref 8. [b] Experimental values compiled in the present study.

free energy of formation of the Al atom only, while the second one uses experimental values for both the Al atom and the Al dimer. Here, we present the results obtained using the second method (in Table 11). The results obtained using the first method are in Supporting Information.

7. Conclusions

We developed two thermodynamic and statistical mechanical methods to calculate the standard Gibbs free energy changes for the growth reactions of Al particles using realistic analytic

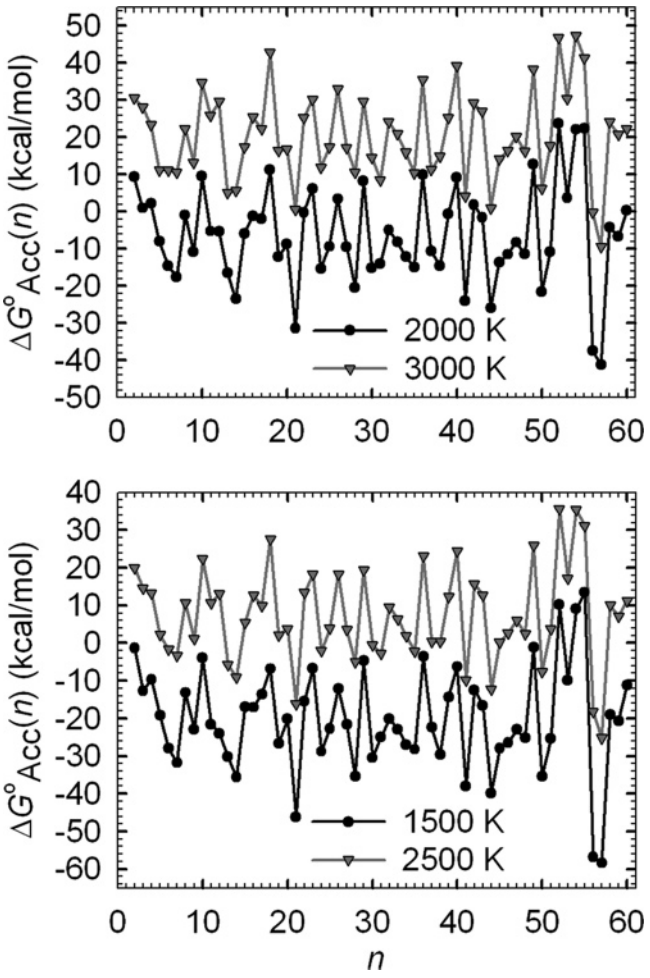

Figure 12. Accurate standard Gibbs free energy change of R1 (kcal/mol) at 1500 K, 2000, 2500, and 3000 K.

potential energy functions, in particular, a method based on Monte Carlo configuration integral (MCCI) integration to obtain partition functions and a method based on a Monte Carlo direct simulation of the equilibrium constants (MCEC). We apply these methods using several well-validated analytic potentials, namely, NP-A, NP-B, NP-A-2347, and NP-B-2347. For the small Al_n clusters with $n = 2-4$, the two completely different approaches agree very well with each other when the same analytic potential function is used. This validates our programs for calculating these quantities, and to the extent that validation at small n is applicable to the large particles, it also validates our methods. However, different potential energy functions yield quantitatively different values of the equilibrium constants and thus free energy changes. Three correction terms, one for the potential energy difference ($\Delta\Delta E_e^{HLC}$), one for the electronic excitation contribution (ΔG_{Elec}), and one for the isomeric−rovibrational contribution (ΔG_{IsoRov}^{HLC}), are proposed to correct the results obtained directly from the simulations to give more accurate results; the first is for potential function accuracy, and the others include quantum effects on vibrations and electronic states. The final results for the dimer formation, which depend very weakly on the potential, are compared to the accurate experimental result, and the agreement is very good.

For reactions involving particle sizes larger than $n = 4$, MCCI is not efficient. So, classical canonical Monte Carlo simulations are performed. To improve the sampling of particles of different sizes, aggregation-volume bias moves are utilized. It is observed that the standard Gibbs free energy change tends toward a plateau value for larger particles, and for a given particle size it increases monotonically with the temperature.

After the high-level corrections are added, we obtain our final estimates of the standard Gibbs free energy changes of R1. These values have been used to calculate the standard Gibbs free energy of formation of Al_n particles with $n = 2-60$. These have never previously been measured or even inferred from a combination of experiments before, nor have standard Gibbs free energies of formation ever been computed for nanoparticles. This is the first example of the systematic creation of thermodynamic tables for nanoparticles.

Acknowledgment. The authors are grateful to Steven Girshick for stimulating discussions. This work was supported by the National Science Foundation and by the Defense-University Research Initiative in Nanotechnology (DURINT) through a grant managed by the Army Research Office. This research was supported in part by a Molecular Science Computing Facility Computational Grand Challenge grant at the Environmental Molecular Sciences Laboratory of Pacific Northwest National Laboratory, operated by Battelle.

Supporting Information Available: Derivation details of eq 37; newly added structures for refitting the NP-A and NP-B potentials using only Al_2, Al_3, Al_4, and Al_7 subsets; refitted parameters of the NP-A-2347 and NP-B-2347 potentials and their MUEs; isomeric−rovibrational partition function of Al_3 and Al_4; potential energy changes of R1 calculated by different methods; uncorrected standard Gibbs free energy change of R1 using different methods; standard free energy of formation of Al_n particles using only experimental data for Al monomer in eq 1; one σ error of the free energy changes in Table 10; thermodynamic functions of Al_2; $\Delta G_{IsoRov}^{HLC}(n)$ calculated with three different ω_{cut}; and plots of the uncorrected standard free energy changes calculated by the AVBMC methods at 2000 and 2500 K. This material is available free of charge via the Internet at http://pubs.acs.org.

References and Notes

(1) Feildheim, D. L.; Foss, C. A. *Metal Nanoparticles: Synthesis, Characterization, and Applications;* Marcel Dekker: New York, 2002.

(2) Schmid, G. *Nanoparticles: From Theory to Applications*; Wiley-VCH: Weinheim, Germany, 2004.

(3) Ramaswamy, A. L.; Kaste, P.; Trevino, S. F. *J. Energ. Mater.* **2004**, *21*, 1−24; Ramaswamy, A. L.; Kaste, P. *J. Energ. Mater.* **2005**, *23*, 1−25.

(4) Galfetti, L.; De Luca, L. T.; Severini, F.; Meda, L.; Marra, G.; Marchetti, M.; Regi, M.; Bellucci, S. *J. Phys.: Condens. Matter* **2006**, *18*, S1991−S2005.

(5) Ivanov, Y. F.; Osmonoliev, M. N.; Sedoi, V. S.; Arkhipov, V. A.; Bondarchuk, S. S.; Vorozhtsov, A. B.; Korotkikh, A. G.; Kuznetsov, V. T. *Propellants, Explos., Protech.* **2006**, *28*, 319.

(6) Züttel, A.; Wenger, P.; Sudan, P.; Mauron, P.; Orimo, S. *Mater. Sci. Eng., B* **2004**, *108*, 9.

(7) Jasper, A. W.; Schultz, N. E.; Truhlar, D. G. *J. Phys. Chem. B* **2005**, *109*, 3915.

(8) Chase, M. W. *NIST-JANAF Thermochemical Tables*, 4th ed.; *J. Phys. Chem. Ref. Data, Monograph 9*, **1998**, 1−1951.

(9) Adamo, C.; Barone, V. *J. Chem. Phys.* **1999**, *110*, 6158.

(10) Jasper, A. W.; Staszewski, P.; Staszewska, G.; Schultz, N. E.; Truhlar, D. G. *J. Phys. Chem. B* **2004**, *108*, 8996.

(11) Schultz, N. E.; Staszewska, G.; Staszewski, P.; Truhlar, D. G. *J. Phys. Chem. B* **2004**, *108*, 4850.

(12) Bhatt, D.; Jasper, A. W.; Schultz, N. E.; Siepmann, J. I.; Truhlar, D. G. *J. Am. Chem. Soc.* **2006**, *128*, 4224. Bhatt, D.; Jasper, A. W.; Schultz, N. E.; Siepmann, J. I.; Truhlar, D. G. *J. Phys. Chem. B* **2006**, *110*, 26135.

(13) Hill, T. L. *An Introduction to Statistical Thermodynamics*; Addison-Wesley: Reading, MA, 1960; p 149.

(14) McQuarrie, D. A. *Statistical Mechanics*; Harper & Row: New York, 1975.
(15) Berry, R. S.; Rice, S. A.; Ross, J. *Physical Chemistry*, 2nd ed.; Oxford University Press: New York, 2000; p 570.
(16) Li, Z. H.; Jasper, A. W.; Truhlar, D. G. *J. Am. Chem. Soc*. 2007, submitted.
(17) Dardi, P. S.; Dahler, J. S. *J. Chem. Phys.* **1990**, *93*, 3562.
(18) Topper, R. Q.; Truhlar, D. G. *J. Chem. Phys.* **1992**, *97*, 3647.
(19) Srinivasan, J.; Volobuev, Y. L.; Mielke, S. L.; Truhlar, D. G. *Comput. Phys. Commun.* **2000**, *128*, 446.
(20) Mielke, S. L.; Srinivasan, J.; Truhlar, D. G. *J. Chem. Phys.* **2000**, *112*, 8758.
(21) Mielke, S. L.; Lynch, V. A.; Truhlar, D. G. *FPIMC, version 26.0;* University of Minnesota: Minneapolis, MN, 2004.
(22) Chen, B.; Siepmann, J. I. *J. Phys. Chem. B* **2000**, *104*, 8725.
(23) Chen, B.; Siepmann, J. I. *J. Phys. Chem. B* **2001**, *105*, 11275.
(24) ten Wolde, P. R.; Frenkel, D. *J. Chem. Phys.* **1998**, *109*, 9901.
(25) Chen, B.; Siepmann, J. I.; Oh, K. J.; Klein, M. L. *J. Chem. Phys.* **2001**, *115*, 10903.
(26) Chen, B.; Siepmann, J. I.; Klein, M. L. *J. Phys. Chem. A* **2005**, *109*, 1137.
(27) Feller, D. *J. Chem. Phys.* **1993**, *98*, 7059.
(28) Lynch, B. J.; Zhao, Y.; Truhlar, D. G. *J. Phys. Chem. A* **2003**, *107*, 1384.
(29) Schultz, N. E.; Truhlar, D. G. *J. Chem. Theory Comp.* **2005**, *1*, 41.
(30) Jones, R. O. *Phys. Rev. Lett.* **1991**, *67*, 224. Jones, R. O. *J. Chem. Phys.* **1993**, *99*, 1194.
(31) Ahlrichs, R.; Elliott, S. D. *Phys. Chem. Chem. Phys.* **1999**, *1*, 13.
(32) Rao, B. K.; Jena, P. *J. Chem. Phys.* **1999**, *111*, 1890.
(33) Chuang, F.-C.; Wang, C. Z.; Ho, K. H. *Phys. Rev. B* **2006**, *73*, 125431.
(34) Bauernschmitt, R.; Ahlrichs R. *Chem. Phys. Lett.* **1996**, *256*, 454.
(35) Wasserman, E.; Stixrude, L.; Cohen, R. E. *Phys. Rev. B* **1996**, *53*, 8296.
(36) Cohen, R. E.; Gülseren, O. *Phys. Rev. B* **2001**, *63*, 224101.
(37) Srepusharawoot, P.; Pinsook, U. *Phys. Stat. Sol.* **2005**, *242*, 1598.
(38) Stratmann, R. E.; Scuseria, G. E.; Frisch, M. J. *J. Chem. Phys.* **1998**, *109*, 8218.
(39) Casida, M. E.; Jamorski, C. K.; Casida, C.; Salahub, D. R. *J. Chem. Phys.* **1998**, *108*, 4439.
(40) Frisch, M. J.; Trucks, G. W.; Schlegel, H. B.; Scuseria, G. E.; Robb, M. A.; Cheeseman, J. R.; Montgomery, J. A., Jr.; Vreven, T.; Kudin, K. N.; Burant, J. C.; Millam, J. M.; Iyengar, S. S.; Tomasi, J.; Barone, V.; Mennucci, B.; Cossi, M.; Scalmani, G.; Rega, N.; Petersson, G. A.; Nakatsuji, H.; Hada, M.; Ehara, M.; Toyota, K.; Fukuda, R.; Hasegawa, J.; Ishida, M.; Nakajima, T.; Honda, Y.; Kitao, O.; Nakai, H.; Klene, M.; Li, X.; Knox, J. E.; Hratchian, H. P.; Cross, J. B.; Bakken, V.; Adamo, C.; Jaramillo, J.; Gomperts, R.; Stratmann, R. E.; Yazyev, O.; Austin, A. J.; Cammi, R.; Pomelli, C.; Ochterski, J. W.; Ayala, P. Y.; Morokuma, K.; Voth, G. A.; Salvador, P.; Dannenberg, J. J.; Zakrzewski, V. G.; Dapprich, S.; Daniels, A. D.; Strain, M. C.; Farkas, O.; Malick, D. K.; Rabuck, A. D.; Raghavachari, K.; Foresman, J. B.; Ortiz, J. V.; Cui, Q.; Baboul, A. G.; Clifford, S.; Cioslowski, J.; Stefanov, B. B.; Liu, G.; Liashenko, A.; Piskorz, P.; Komaromi, I.; Martin, R. L.; Fox, D. J.; Keith, T.; Al-Laham, M. A.; Peng, C. Y.; Nanayakkara, A.; Challacombe, M.; Gill, P. M. W.; Johnson, B.; Chen, W.; Wong, M. W.; Gonzalez, C.; Pople, J. A. *Gaussian 03*, revision C.02; Gaussian, Inc.: Wallingford, CT, 2004.
(41) Mayer, S. W.; Schieler, L.; Johnston, H. S. *J. Chem. Phys.* **1966**, *45*, 385.
(42) Bylaska, E. J.; de Jong, W. A.; Kowalski, K.; Straatsma, T. P.; Valiev, M.; Wang, D.; Aprà, E.; Windus, T. L.; Hirata, S.; Hackler, M. T.; Zhao, Y.; Fan, P.-D.; Harrison, R. J.; Dupuis, M.; Smith, D. M. A.; Nieplocha, J.; Tipparaju, V.; Krishnan, M.; Auer, A. A.; Nooijen, M.; Brown, E.; Cisneros, G.; Fann, G. I.; Früchtl, H.; Garza, J.; Hirao, K.; Kendall, R.; Nichols, J. A.; Tsemekhman, K.; Wolinski, K.; Anchell, J.; Bernholdt, D.; Borowski, P.; Clark, T.; Clerc, D.; Dachsel, H.; Deegan, M.; Dyall, K.; Elwood, D.; Glendening, E.; Gutowski, M.; Hess, A.; Jaffe, J.; Johnson, B.; Ju, J.; Kobayashi, R.; Kutteh, R.; Lin, Z.; Littlefield, R.; Long, X.; Meng, B.; Nakajima, T.; Niu, S.; Pollack, L.; Rosing, M.; Sandrone, G.; Stave, M.; Taylor, H.; Thomas, G.; van Lenthe, J.; Wong, A.; Zhang, Z. *NWChem, A Computational Chemistry Package for Parallel Computers, Version 5.0;* Pacific Northwest National Laboratory: Richland, Washington, 2006.
(43) Werner, H.-J.; Knowles, P. J.; Lindh, R.; Schtz, M.; Celani, P.; Korona, T.; Manby, F. R.; Rauhut, G.; Amos, R. D.; Bernhardsson, A.; Berning, A.; Cooper, D. L.; Deegan, M. J. O.; Dobbyn, A. J.; Eckert, F.; Hampel, C.; Hetzer, G.; Lloyd, A. W.; McNicholas, S. J.; Meyer, W.; Mura, M. E.; Nick-lass, A.; Palmieri, P.; Pitzer, R.; Schumann, U.; Stoll, H.; Stone, A. J.; Tarroni, R.; Thorsteinsson, T. *MOLPRO, version 2002.8, A Package of Ab Initio Programs*; University College Cardiff Consultants Limited, 2003.
(44) Lynch, V. A.; Mielke, S. L.; Truhlar, D. G. *J. Chem. Phys.* **2004**, *121*, 5148.
(45) Martin, W. C.; Zalubas, R. *J. Phys. Chem. Ref. Data* **1979**, *8*, 817.
(46) Chase, J.; M. W.; Davies, C. A.; Downey, J. J. R.; Frurip, D. J.; McDonald, R. A.; Syverud, A. N. *JANAF thermochemical tables*, 3rd ed.; American Chemical Society and the American Institute of Physics for the National Bureau of Standards: Washington, D.C., 1986.
(47) Zeeman, P. B. *Can. J. Phys.* **1954**, *32*, 9.
(48) Fu, Z. W.; Lemire, G. W.; Bishea, G. A.; Morse, M. D. *J. Chem. Phys.* **1990**, *93*, 8420.
(49) Woon, D. E.; Dunning, T. H. *J. Chem. Phys.* **1994**, *101*, 8877.
(50) Stearns, C. A.; Kohl, F. J. *High Temp. Sci.* **1973**, *5*, 113.
(51) Lewis, G. N.; Randall, M. *Thermodynamics*, 2nd ed.; McGraw-Hill: New York, 1961; revised by Pitzer, S. K.; Brewer, L.
(52) Martinez, A.; Vela, A.; Salahub, D. R.; Calaminici, P.; Russo, N. *J. Chem. Phys.* **1994**, *101*, 10677; Martinez, A.; Vela, A.; Salahub D. R. *Int. J. Quantum Chem.* **1997**, *63*, 301.
(53) Geske, G. D.; Alexander, I.; Boldyrev, A. I.; Li, X.; Wang, L. S. *J. Chem. Phys.* **2000**, *113*, 5180.
(54) Pushpa, R.; Narasimhan, S.; Waghmare, U. *J. Chem. Phys.* **2004**, *121*, 5211.